nature neuroscience

RESOURCE

https://doi.org/10.1038/s41593-021-00905-6

Neuroinflammatory astrocyte subtypes in the mouse brain

Philip Hasel[1]✉, Indigo V. L. Rose[1], Jessica S. Sadick[1], Rachel D. Kim[1] and Shane A. Liddelow[1,2,3]✉

Astrocytes undergo an inflammatory transition after infections, acute injuries and chronic neurodegenerative diseases. How this transition is affected by time and sex, its heterogeneity at the single-cell level and how sub-states are spatially distributed in the brain remains unclear. In this study, we investigated transcriptome changes of mouse cortical astrocytes after an acute inflammatory stimulus using the bacterial cell wall endotoxin lipopolysaccharide. We identified fast transcriptomic changes in astrocytes occurring within hours that drastically change over time. By sequencing ~80,000 astrocytes at single-cell resolution, we show that inflammation causes a widespread response with subtypes of astrocytes undergoing distinct inflammatory transitions with defined transcriptomic profiles. We also attribute key sub-states of inflammation-induced reactive astrocytes to specific brain regions using spatial transcriptomics and in situ hybridization. Together, our datasets provide a powerful resource for profiling astrocyte heterogeneity and will be useful for understanding the biological importance of regionally constrained reactive astrocyte sub-states.

Astrocytes perform crucial homeostatic functions such as neurotransmitter uptake and recycling of metabolites to support active neurons[1,2] and form an integral part of the blood–brain barrier protecting the brain from toxic metabolites and peripheral insults[3]. They also undergo inflammatory transitions after acute insults like stroke[4] and spinal cord injury[5], as well as in chronic diseases like Alzheimer's disease, and during normal ageing[6–8]. This 'reactive' response depends on the initiating insult[4,6]. For example, systemic inflammation causes a neurotoxic reactive subtype induced by microglial cytokine release[6]. However, whether this inflammatory insult induces a single homogeneous population or other multiple heterogeneous astrocyte subsets is not known. Recent work has shown that astrocytes have distinct gene expression profiles depending on brain region or cortical layer[9–14]. Similarly, the astrocytic transcriptome can be affected by neuronal contact or neuronal activity[15]. We decided to investigate whether astrocyte heterogeneity is maintained during responses to inflammation and if additional layers of heterogeneity are present.

We induced systemic inflammation in mice using the endotoxin lipopolysaccharide (LPS) and used a multimodal approach consisting of in vitro and in vivo bulk RNA-sequencing (RNA-seq), single-cell RNA-seq (scRNA-seq), spatial transcriptomics, NanoString gene profiling and dataset integration to profile the astrocytic response to an inflammatory insult. These data provide valuable insights to the temporal, spatial and single-cell responses of astrocytes to inflammation and give insights into the evolution of heterogeneous responses of astrocyte to a single stimulus while simultaneously highlighting some degree of homogeneity across astrocyte subtypes.

Results

Astrocytes acquire distinct inflammatory states over time. To investigate astrocytic time-dependent transcriptome changes to inflammation, we injected postnatal day 30–35 (P30–35) *Aldh1l1*^{eGFP} reporter mice intraperitoneally with LPS or endotoxin-free saline as control. Although LPS does not cross the blood–brain barrier extensively[16], it mounts an inflammatory response in microglia required to induce astrocyte reactivity[6]. Three, 24 and 72 h after LPS injection, cortical astrocytes were fluorescence-activated cell sorting (FACS) purified, and total RNA was extracted and processed for bulk RNA-seq (Fig. 1a and Extended Data Fig. 1a). We found extensive changes in astrocytic gene expression at 3 h (383 Up, 128 Down), 24 h (442 Up, 158 Down) and 72 h (126 Up, 4 Down) (Fig. 1b,c and Supplementary Table 1). The response at 24 h was similar to that published previously[4], with common astrocyte reactivity markers *Gfap* and *Serpina3n* upregulated at all time points (Fig. 1e, Supplementary Table 2 and Supplementary Table 3). We found, however, that changes in gene expression were mostly unique to individual time points (Fig. 1d and Supplementary Table 2), with only 4% of 743 altered genes induced across all time points. For example, interferon stimulated genes (ISGs) such as *Iigp1*, *Cxcl10* and *Gbp2* are expressed highest at 3 h (Fig. 1e,f and Supplementary Table 2). At 24 h, genes involved in angiogenesis and blood pressure like *Fbln5, Agt* and genes involved in extracellular matrix remodeling including *Timp1* are upregulated (Fig. 1e,f and Extended Data Fig. 2). In particular, *Fbln5* is interesting given its involvement in cell adhesion and vascular constriction during inflammation[17]. To contextualize these changes in terms of (probable) function, we used the Gene Ontology (GO) tool Metascape[18] (Extended Data Fig. 2 and Supplementary Table 3). We found unique and shared GO terms across all time points (Extended Data Fig. 2 and Supplementary Table 3). Examples of shared GO terms include 'adaptive immune response', 'NF-kappa B signaling pathway' and 'response to type I interferons'. We also found GO terms specific for each time point, which, at 3 h, included 'positive regulation of interleukin-12 production', 'interleukin-1 mediated signaling pathway' and 'interferon-gamma production'. At 24 h, these included 'regulation of coagulation', 'tissue remodeling' and 'antigen processing

[1]Neuroscience Institute, NYU Grossman School of Medicine, New York, NY, USA. [2]Department of Neuroscience & Physiology, NYU Grossman School of Medicine, New York, NY, USA. [3]Department of Ophthalmology, NYU Grossman School of Medicine, New York, NY, USA. ✉e-mail: philip.hasel@nyulangone.org; shane.liddelow@nyulangone.org

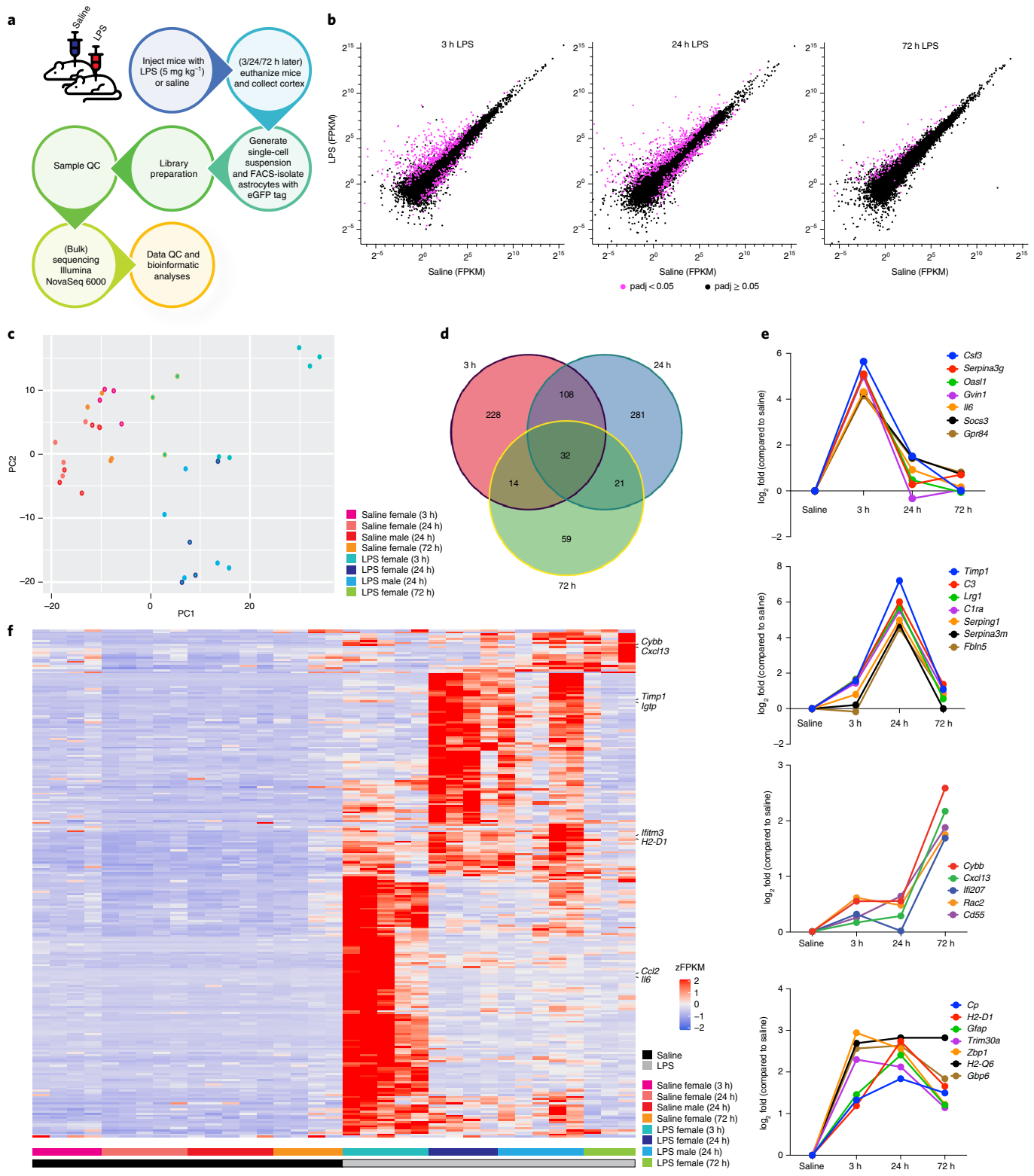

Fig. 1 | Astrocytes undergo a fast inflammatory transition that drastically changes over time. a, Schematic of experimental approach for astrocyte bulk sequencing of saline- and LPS-injected *Aldh1l1*^{eGFP} mice. **b**, FPKM scatter plots of all analyzed genes of FACS-purified astrocytes comparing saline- to LPS-injected female mice at 3 h, 24 h and 72 h after injection. Genes highlighted in purple are $P_{adj} < 0.05$, saline 3 h ($n = 4$ animals), 24 h ($n = 5$), 72 h ($n = 4$) and LPS 3 h ($n = 5$), 24 h ($n = 4$) and 72 h ($n = 3$). **c**, PCA of samples in **b** and saline- and LPS-injected male mice at 24 h after injection (saline $n = 5$, LPS $n = 5$). **d**, Venn diagram of genes induced ≥1 $\log_2$ fold with $P_{adj} < 0.05$ in any of three time points (female mice). **e**, $\log_2$ fold induction of genes primarily induced at 3 h (top panel), 24 h (second panel) or 72 h (third panel) as well as genes significantly upregulated at all three time points (bottom panel), all female. **f**, Heat map of genes strongly induced (≥2 $\log_2$ fold with $P_{adj} < 0.05$, z-transformed FPKM values) in any of the three time points and clustered according to the induction pattern over time, all three time points of female mice plus the 24-h injection time point for male mice.

and presentation of endogenous peptide antigen via MHC class I via ER pathway'. GO terms specific to 72 h included 'regulation of humoral immune response mediated by circulating immunoglobulin', 'response to triacyl bacterial lipopeptide' and 'mast cell activation' (Extended Data Fig. 2 and Supplementary Table 3).

We next asked if sex-specific gene expression changes occur in astrocytes during inflammation. We compared transcriptomes of female and male mice at baseline and 24 h after LPS injection. In a physiological setting, there were only ten differentially expressed genes (DEGs) between female and male astrocytes, with most either Y-linked (for example, *Eif2s3y*) or X-linked (for example, *Xist*) (Extended Data Fig. 7 and Supplementary Table 8), suggesting astrocytes are homogeneous across sexes during normal physiology. To find sex-specific DEGs, we searched for genes induced ($P_{adj} < 0.05$ based on DESeq2) in only one sex after LPS injection, which were also significantly different when comparing LPS-treated female versus LPS-treated male mice. Using this stringent approach, we found 39 DEGs specific to male mice (28 Up, 11 Down) and 14 genes specific to female mice (8 Up, 6 Down) (Supplementary Table 8). As examples, *Far1*, *Cdh19* and *Tsc22d3* were only induced in female mice (Extended Data Fig. 7 and Supplementary Table 8). Of note, *Tsc22d3* is an X-linked gene that can be induced by glucocorticoids and is ascribed anti-inflammatory properties[19,20].

Complex astrocyte subsets occupy distinct areas in the brain. To further understand astrocytic heterogeneity, we next performed scRNA-seq on FACS-purified astrocytes from LPS- and saline-injected male and female *Aldh1l1*^{eGFP} mice (Fig. 2a and Extended Data Fig. 1). Astrocytes were collected 24 h after injection and individual cells captured using the 10x Chromium platform, libraries prepared and sequencing completed on the Illumina NovaSeq 6000 platform. Data were quality checked and analyzed following *muscat* and *seurat* pipelines (Methods)[21–23].

After removing non-astrocytic cells using cell type markers (Extended Data Fig. 1b,c and Supplementary Table 4), 79,944 astrocytes expressing classical astrocytic marker genes (for example, *Apoe*, *Gfap*, *Aqp4* and *Slc1a3*) remained, with a median of 1,257 genes per cell (Fig. 1a and Extended Data Figs. 3 and 10). Ten clusters were identified (Fig. 2b,c and Supplementary Tables 4 and 5). These clusters express new and previously identified marker genes and are partly informed by layer-specific genes. For example, Cluster 1 expresses upper cortical layer enriched markers *Mfge8* and *Igfbp2* (ref. [10]), and Cluster 2 expresses *Nnat*, *Dbi*, and *Agt*, which have previously been reported to show layer-specific expression in astrocytes[11]. Similarly to Cluster 1, Cluster 3 expresses the general gray matter gene *Igfbp2* (ref. [10]) as well as *Nupr1* and *Thrsp*. Cluster 4 expresses classical white matter genes *Vim* and *Gfap* in the control brain but is primarily defined by inflammatory markers including *Lcn2*, *Ifitm3* and *Timp1* after inflammation. Cluster 5 astrocytes are enriched for *Slc43a3*, *Prss56* and *Crym*, which are reported in subventricular zone (SVZ)[24] and striatal astrocytes[9]. Cluster 6 expressed high levels of *Gfap* in control brain, the synaptogenic marker *Thbs4* (ref. [25]), as well as *Igfbp5*, *Fxyd6* and the white matter gene *Cd9*. Cluster 7 expressed another synapto-modulatory gene, *Sparc*[26], the AMPA receptor subunit *Gria1* and the classically oligodendrocyte-associated gene *Nkx6-2*. Cluster 8, which is almost exclusively present in the inflamed brain, is enriched in ISGs such as *Igtp*, *Ifit3* and *Iigp1*. Lastly, *Zic1*, *Slc38a1, Hopx* and *Col1a2* defined Cluster 9, a subset also reported in the SVZ[24]. Given that these clusters are at least partly defined by layer-specific or layer-enriched genes, we compared our dataset to the Bayraktar et al. dataset[10]. We find that, in general, our clusters fall into either gray matter/upper layer enriched (Clusters 0, 1, 3 and 8) or white matter/deep layer/subpial (Clusters 2, 4, 5, 6, 7 and 9) (Extended Data Fig. 5a–c).

To identify whether our astrocyte clusters occupy distinct anatomical locations, we next performed spatial transcriptomics on brain sections from three saline-treated and three LPS-treated mice using Visium from 10x Genomics. Although Visium does not provide single-cell resolution, we were able to query both astrocyte-specific genes such as *Gfap*, *S100b* or *Aldh1l1*, as well as 'modules' of genes (Fig. 2d and Extended Data Fig. 4). By creating modules for each cluster from our scRNA-seq experiments, we approximated their location in brain sections. We validated this approach by highlighting layer-specific pyramidal neuron genes (as assessed by scRNA-seq in Zeisel et al.[12]) and show that we can reliably highlight different cortical layers (Extended Data Fig. 5d). Additionally, we show the location of white matter tracts by highlighting the highly expressed and oligodendrocyte-specific gene *Mbp* (Extended Data Fig. 5e).

As our scRNA-seq experiments investigated only astrocytes from cortex and underlying white matter tracts, we sought to validate their location in distinct anatomical locations in agreement with cortical layer-specific astrocytes (Fig. 2d and Extended Data Fig. 5a–c). For example, Cluster 4, which expresses deep layer gene *Id3*, and Cluster 6, which expresses deep layer gene *Cd9*, both track *Gfap*^{high} white matter tracts and are present just below the pia. Indeed, subpial and deep Layer 6 astrocytes have characteristics of white matter astrocytes (Extended Data Fig. 5a–c). Cluster 3 conversely expresses gray matter marker *Igfbp2* and Layer 2/3 marker *Nupr1* and is located in mid-layer cortical gray matter but is also present in sub-cortical gray matter. Cluster 9 astrocytes surround the third ventricle and are *Zic1*$^{+}$/*Hopx*$^{+}$ and have been reported around the SVZ[24]. Like Cluster 9, Cluster 1 expresses the upper layer-biased gene *Mfge8*, and we found it enriched in Layer 1. Cluster 2 occupies white matter tracts as well as subpial areas of the brain confirming that *Nnat* and *Agt* are deep layer/white matter as well as subpial genes. However, Cluster 2 is also present in the hippocampus, similarly to Cluster 3 and 5. Cluster 5 also expresses Layer 6 genes *Dkk3*, *Cst3* and *Lxn*, and is localized in lower cortical layers in our Visium data. Cluster 8 is expressed at very low levels in control animals, as was expected given our scRNA-seq data, and its expression only becomes apparent in the inflamed brain.

The response of astrocytes to inflammation is heterogeneous. To understand how individual clusters respond to LPS-induced inflammation, we next identified cluster-specific DEGs. We employed the scRNA-seq tool *muscat*[23], which uses a pseudobulk approach to perform multi-sample, multi-condition, cluster-specific DEG analysis (Fig. 3a–c). We observed that all clusters responded robustly to LPS-induced inflammation (Fig. 3b–d and Supplementary Table 6). Comparing astrocytes from saline- to LPS-injected mice, we found 68% of all astrocytes from LPS-stimulated mice expressed

Fig. 2 | Astrocytic subtypes as identified by single-cell RNA-seq and localized using spatial transcriptomics in the brain of saline-treated mice. **a**, Schematic of experimental approach for astrocyte single-cell RNA-seq and spatial transcriptomics of saline- and LPS-injected *Aldh1l1*^{eGFP} mice. **b**, After removal of non-astrocytic cells, 79,944 astrocytes were re-clustered based on variable features calculated for each sample and used to anchor the 12 samples. t-SNE plots are split across all four conditions: Female saline, male saline, female LPS and male LPS (left to right, $n = 3$ animals each). Colors highlight the ten identified astrocyte clusters. **c**, Genes statistically enriched in each cluster using *seurat's* FindAllClusters function. Shown is the normalized average expression of the top enriched genes for each cluster. **d**, Visium spatial transcriptomics highlights classical astrocyte-specific markers in one of the six coronal brain sections (here, saline-treated) as well as showing the expression of astrocyte clusters identified using single-cell RNA-seq using a module-based approach.

Serpina3n, the most widely LPS-induced gene, compared to 3% of astrocytes from saline-treated animals. Although most astrocytes show overlapping gene inductions, different clusters mount different inflammatory responses (Fig. 3c,d and Supplementary Table 6). We found uniquely induced genes for each cluster, with Cluster 4 having the most cluster-specific DEGs (36) followed by Cluster 8 with 18

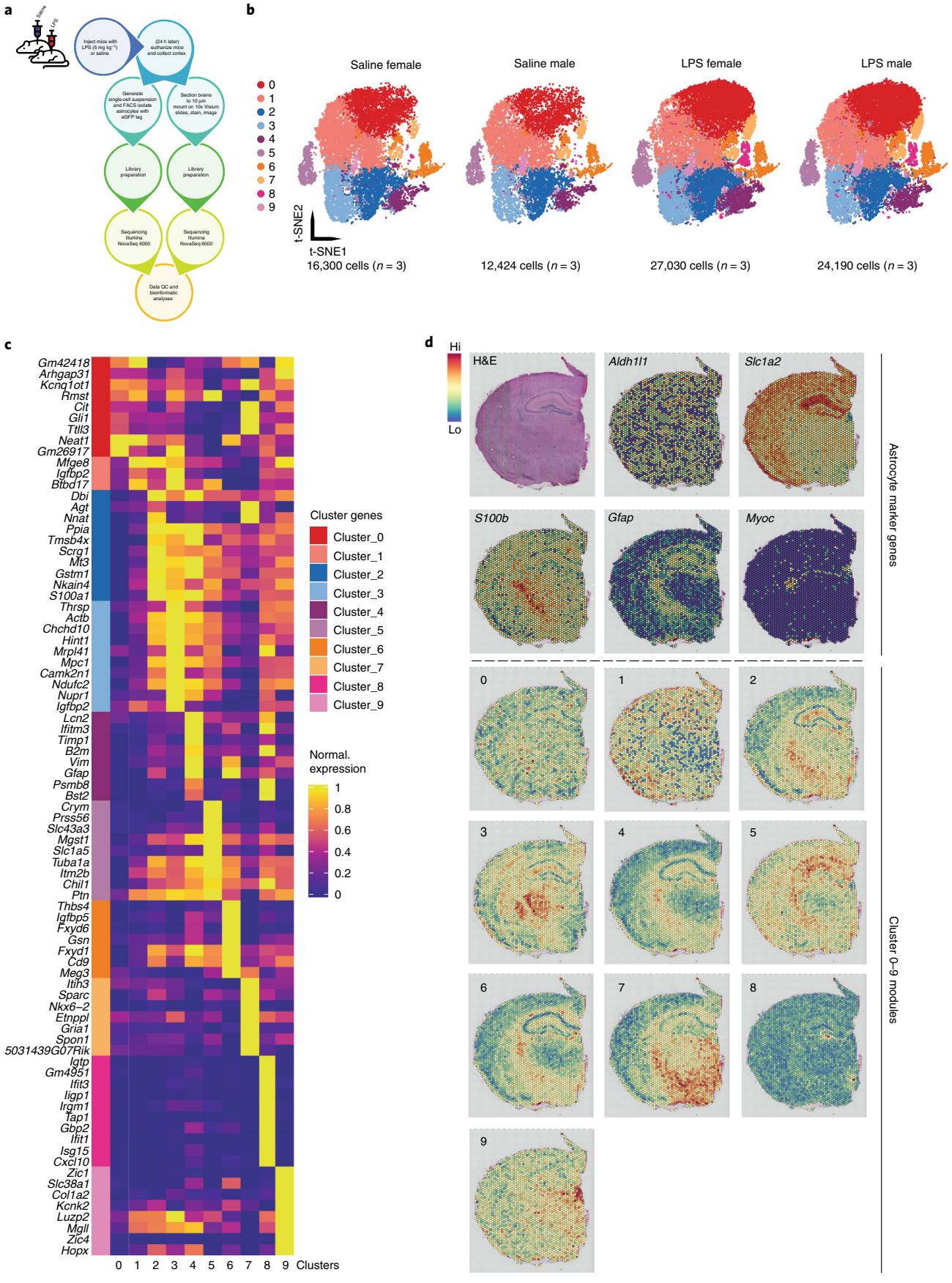

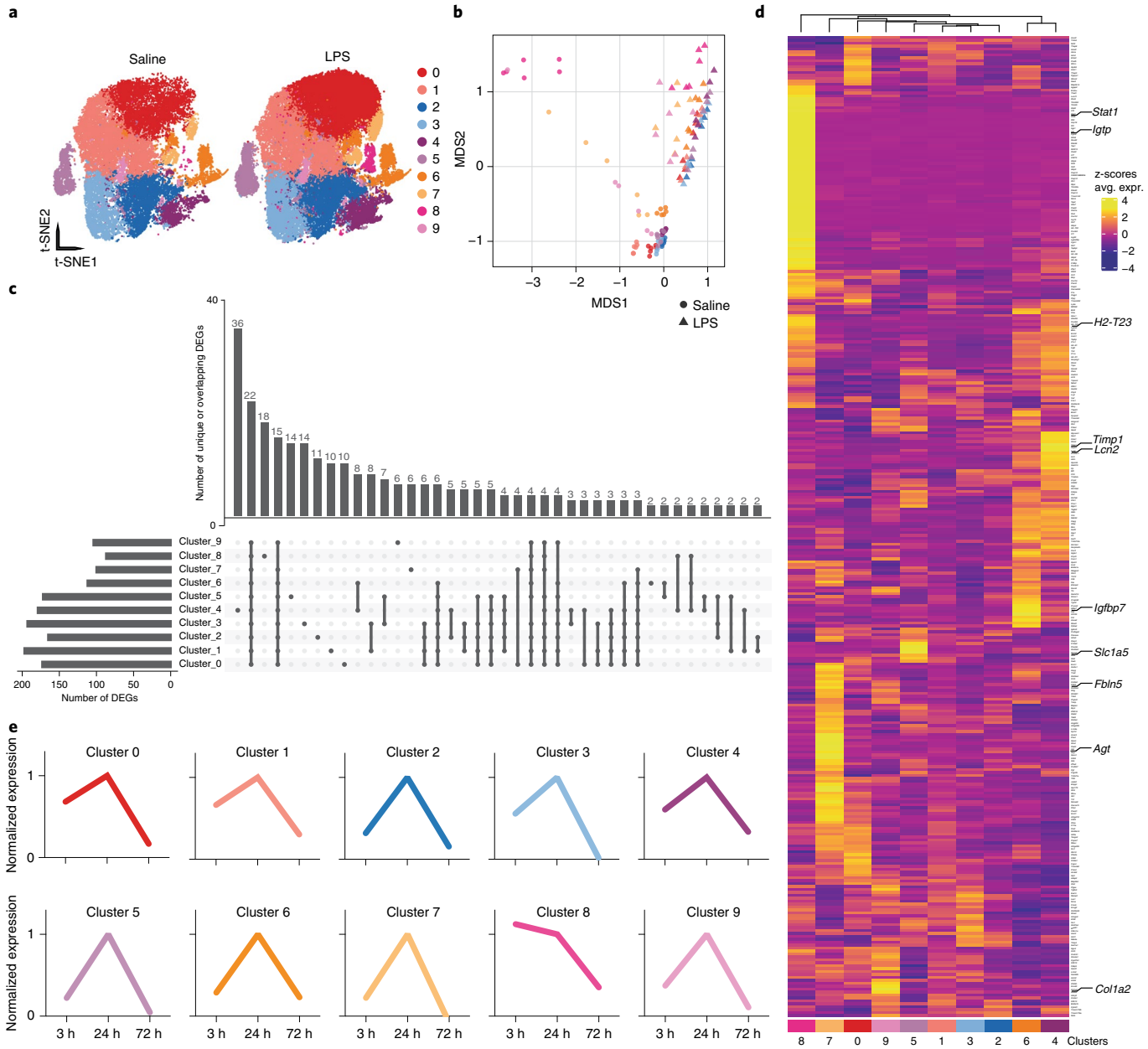

Fig. 3 | Inflammation causes a heterogenous, subtype-specific reactive transcriptomic response in astrocytes. a, t-SNE projection of 79,944 astrocytes split into saline- and LPS-injected mice. **b**, Multidimensional scaling (MDS) plot of pseudobulk counts showing pairwise distances of each sample and their clusters in saline- and LPS-injected animals. **c**, UpSet plot showing unique and overlapping DEGs for each cluster as calculated using *muscat*'s pseudobulk DEG analysis. **d**, Heat map showing cluster-enriched LPS-induced genes. z-transformed cluster average of astrocytic LPS-induced genes across all ten clusters highlights cluster-specific inflammatory gene expression. Genes of interest are highlighted. **e**, Modules of cluster-enriched LPS-responsive genes from **d** show cluster-resolved inflammatory transition over time and highlight the early response of Cluster 8.

(Fig. 3c). Most genes, however, show a complex co-regulation across clusters, with 45 DEGs being common among nine clusters (Fig. 3c). When looking at cluster-enrichment for LPS-induced genes, we again observe cluster-specific expression of inflammatory genes. For example, Cluster 8 is enriched for ISGs such as *Igtp*, *Tap1* and *Stat1*. Cluster 7, meanwhile, induces genes involved in angiogenesis, including *Agt*, *Cd34*, *Fbln5* and *Pgf*. Cluster 6 increases expression of *C3* and the C3-like gene encoding *Cd109* (known to suppress TGFb signaling) as well as *Igfbp7* (angiomodulin), an angiocrine factor that antagonizes VEGF-induced vascular permeabilization[27–29]. The *Gfap*^{high} white matter Cluster 4 exhibits a pronounced enrichment for the metalloproteinase inhibitor *Timp1* and a potential protective program consisting of the anti-oxidant glutathione peroxidase *Gpx1*, the neuroprotective heat shock protein *Hspb1* and *Gap43*, which is reported to suppress neurotoxicity[30]. Cluster 5, primarily present in hippocampus and deep cortical layers, is enriched for LPS-induced genes *Slc1a5*, a glutamine transporter, and *Slc43a3*, a nucleobase transporter involved in adenosine transport[31,32].

We next asked how these cluster-enriched inflammatory genes behave over time. We created inflammatory gene modules for each cluster and identified their trajectory using our bulk sequencing data (Fig. 3e). Because our scRNA-seq data were collected at 24 h after LPS injection, it is not surprising that most clusters peak at 24 h. We identify early responders (Clusters 0, 1, 3, 4 and 8) and astrocytes

with resolved inflammatory responses after 72 h (Clusters 3, 4, 5, 7 and 9). Cluster 8 appeared to be the 'fastest' responding cluster, indicating that it is a strong, early interferon-dependent inflammatory astrocytic subset. We also confirm our scRNA-seq and bulk-seq DEG analysis using NanoString on saline- or LPS-treated mice (Extended Data Fig. 8). These data validate that Cluster 8 is a rapid responder with upregulation of many DEGs by 3 h (Extended Data Fig. 8e–l).

Because Cluster 4 showed the most unique DEGs, and Cluster 8 was the most well-defined in terms of inflammatory genes and showed a strong early inflammatory response, we decided to further investigate them. These two populations represent a small percentage of total cortical astrocytes responding to LPS, and we sought to determine if they are located in additional central nervous system (CNS) regions outside the cortex (perhaps in greater abundance), determine any possible mechanisms of activation and investigate if they are also present in chronic disease models where inflammation is a key modulator of pathology.

Reactive subsets of astrocytes occupy distinct anatomical locations. Although all astrocyte clusters responded to LPS, Clusters 4 and 8 have particularly interesting profiles. The white matter cluster Cluster 4 comprised 5.9% of all sequenced astrocytes and is primarily defined by inflammatory markers including *Timp1*, *Gap43*, *Hspb1, Lcn2* and *Gfap*. Cluster 4 also expressed genes typically induced by interferon, including *Psmb8*, *Ifitm3* and genes involved in antigen presentation*: H2-K1*, *H2-T23* and *H2-D1* (Fig. 4a–c and Supplementary Tables 4–6). Using 10x Visium spatial transcriptomics, we find that, both in saline- and LPS-treated animals, Cluster 4 cells were present in *Gfap*$^+$ white matter tracts, including corpus callosum, as well as between the third and lateral ventricles, a tract that is also occupied by *Myoc*$^+$ astrocytes (Figs. 2d and 4d). Although Cluster 4 is identified in the control and inflamed mouse brain, only after LPS injection does it express the inflammatory genes above—validating our earlier finding that LPS-responsive reactive astrocytes do not necessarily lose their physiological identity (Fig. 3 and Supplementary Table 6). When probing for a Cluster 4 gene module, we find robust induction in all Visium brain sections from LPS-treated, but not saline-injected, animals (Fig. 4e and Extended Data Fig. 4h). Beyond the inflammatory gene signature, Cluster 4 is defined by high levels of *Aqp4*, *Gfap* and *Vim* and the deep layer/white matter genes *Id1*, *Id3* and *Id4*. To verify that these are indeed astrocytes, we used RNAscope in situ hybridization to visualize *Timp1* in LPS-treated animals (as *Timp1* was enriched in Cluster 4 astrocytes from LPS-treated animals—Fig. 4f and Extended Data Fig. 6f–j.). We found *Timp1*$^+$ astrocytes in white matter tracts close to the ventricles (Fig. 4g–j and Extended Data Fig. 6f–j), indicating that the inflammatory component of Cluster 4 might be induced by peripheral signals coming through the ventricles. It is worth noting that *Timp1* is not exclusively expressed in Cluster 4 but is highly and selectively enriched in this cluster. Indeed, we find strongly *Timp1*$^+$ astrocytes only in white matter but argue that the identification of Cluster 4 using *Timp1* has to be performed in the context of its anatomical location. Similarly, not all Cluster 4 astrocytes become *Timp1*$^+$ after LPS injection (~40%) and, most importantly, only in astrocytes that surround the ventricles (Fig. 4c,g–j and Extended Data Fig. 6f–j).

Unlike Cluster 4, Cluster 8 shows a strong, early response to LPS and is the only cluster that was almost exclusively present in LPS-treated mice (Fig. 5a,d and Supplementary Table 4). Even in LPS-treated mice, it represented only 2.7% of all sequenced astrocytes (only 1,383 cells in our dataset) and is primarily defined by inflammatory genes. Most of those genes are ISGs, including the master regulators of IFN-dependent transcription, *Stat1* and *Stat2*. Other genes enriched in Cluster 8 include those involved in antigen processing (*Tap1* and *Tap2*) and presentation (*H2-Q4*, *H2-K1*, *H2-Ab1*, *H2-D1* and *H2-T23*) and IFN-induced GTPases (*Gbp3*, *Gbp7*, *Gbp2*, *Irgm1*, *Iigp1* and *Igtp*) (Fig. 5b,c and Supplementary Tables 5 and 6), suggesting that these astrocytes were exposed to interferons and increased antigen-presenting capabilities. When probing for Cluster 8 in LPS-treated mice brains with Visium, we observed a small but specific signal similar to Cluster 4, with high expression around the lateral and third ventricles, in tracts below the hippocampus, as well as sparse signal coming from the brain surface (see below). Unlike Cluster 4, Cluster 8 does not track *Gfap*^{high} white matter regions and does not express any white matter genes but, rather, expresses upper-layer genes (Extended Data Fig. 5a). When probing for inflammatory Cluster 8 genes, we find consistent expression in Visium brain sections from LPS-treated animals but not saline-treated animals (Fig. 5e and Extended Data Fig. 4h). We next used RNAscope to confirm this signal derives from astrocytes by probing for *Igtp*—a DEG specific to Cluster 8 and only present in LPS-treated brains (Fig. 5f). We confirm that *Igtp*$^+$ cells are astrocytes by co-localization with *Slc1a3* (GLAST) and find that Cluster 8 astrocytes are present in Layer 1 of the cortex near the brain surface where often their cell bodies (rather than just their endfeet terminal processes) associate with vessels (Fig. 5g,h and Extended Data Fig. 6a–e). Visium also finds an interferon gene signature around the ventricles and below the hippocampus, an area occupied by *Myoc*$^+$ astrocytes. Although Visium is powerful at detecting overall anatomical patterns of cluster distributions, it fails to detect sparse *Igtp*$^+$ astrocytes near the surface of the brain, which we only detected using RNAscope. Given their location and striking interferon response gene signature, we sought to determine if Cluster 8 astrocytes were induced by interferons or other known inducers of inflammatory reactive astrocytes.

An in vitro model of Cluster 8 astrocytes. We next investigated whether IFN type1 (IFNβ) or IFN type2 (IFNγ) could induce Cluster 8 or whether it is the product of a more complex inflammatory environment. We immunopanned cortical astrocytes and cultured them in the absence of serum to maintain a physiological in vivo gene expression profile[33]. We exposed astrocytes to IFNγ or IFNβ to test if either interferon was sufficient to induce the Cluster 8 gene signature, or the microglia-derived cytokine cocktail of TNF, IL1α and C1q (TIC)[6] to determine if Cluster 8 did not require

Fig. 4 | Cluster 4 is an LPS super-responder that resides in the white matter. a, t-SNE projection with Cluster 4 highlighted, split into saline- and LPS-injected mice. **b**, t-SNE projections highlighting example marker genes for Cluster 4, *Gap43* and *Timp1*, in LPS-treated animals. **c**, Dot plot showing genes enriched in Cluster 4, split into saline- and LPS-injected mice and across all clusters. Saline-injected animals are in light blue; LPS-injected animals are in purple. **d**, Cluster 4 is highlighted in sections from saline- and LPS-treated animals using Visium spatial transcriptomics and modules of Cluster 4 enriched genes. **e**, Quantification of Cluster 4-specific, LPS-induced genes in three saline- and three LPS-injected animals using Visium and modules of LPS-responsive Cluster 4 genes. *P* values calculated with two-tailed *t*-test on spot-averages of inflammatory gene modules. **f**, Cluster average of *Timp1* across saline- and LPS-injected mice. Data points represent animals—six saline- and six LPS-injected animals. Graphs show the mean; error bars are s.e.m. **g**, Schematic showing location of images in **h–j**. **h**, Low magnification of DAPI and *Timp1* showing presence of Cluster 4 astrocytes in white matter tracts above the ventricles (scale bar, 200 µm) **i**, Higher magnification images showing *Timp1*$^+$ and *Slc1a3*$^+$ astrocytes in white matter (scale bar. 25 µm). **j**, Merged image from **i** showing overlap of *Timp1* and *Slc1a3* (scale bar, 25 µm). GM = gray matter, WM = white matter, VN = ventricle. Representative images from four saline- and four LPS-treated animals, but see Extended Data Fig. 7f–j for additional validation.

interferon directly. We also included combinations of both interferons and TIC. We find that both IFNγ and IFNβ, as well as TIC, drive drastic changes in gene expression, with IFNγ inducing 216, IFNβ 363, TIC 824, TIC + IFNγ 1,108 and TIC + IFNβ 1,023 genes (Fig. 6a–c and Supplementary Table 7). IFNγ and IFNβ share 168 induced genes, and, of the 411 genes induced by IFNγ and/or IFNβ,

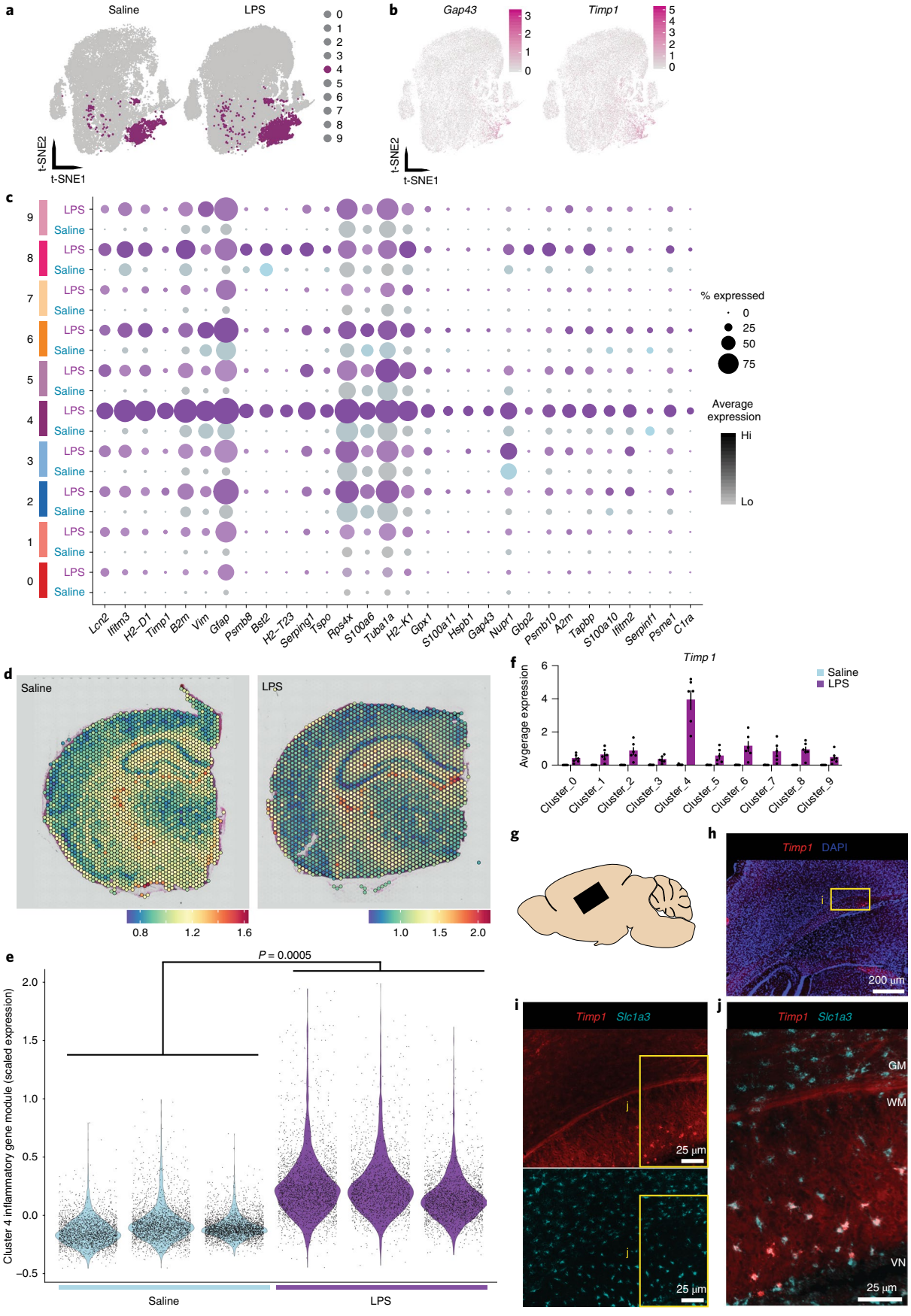

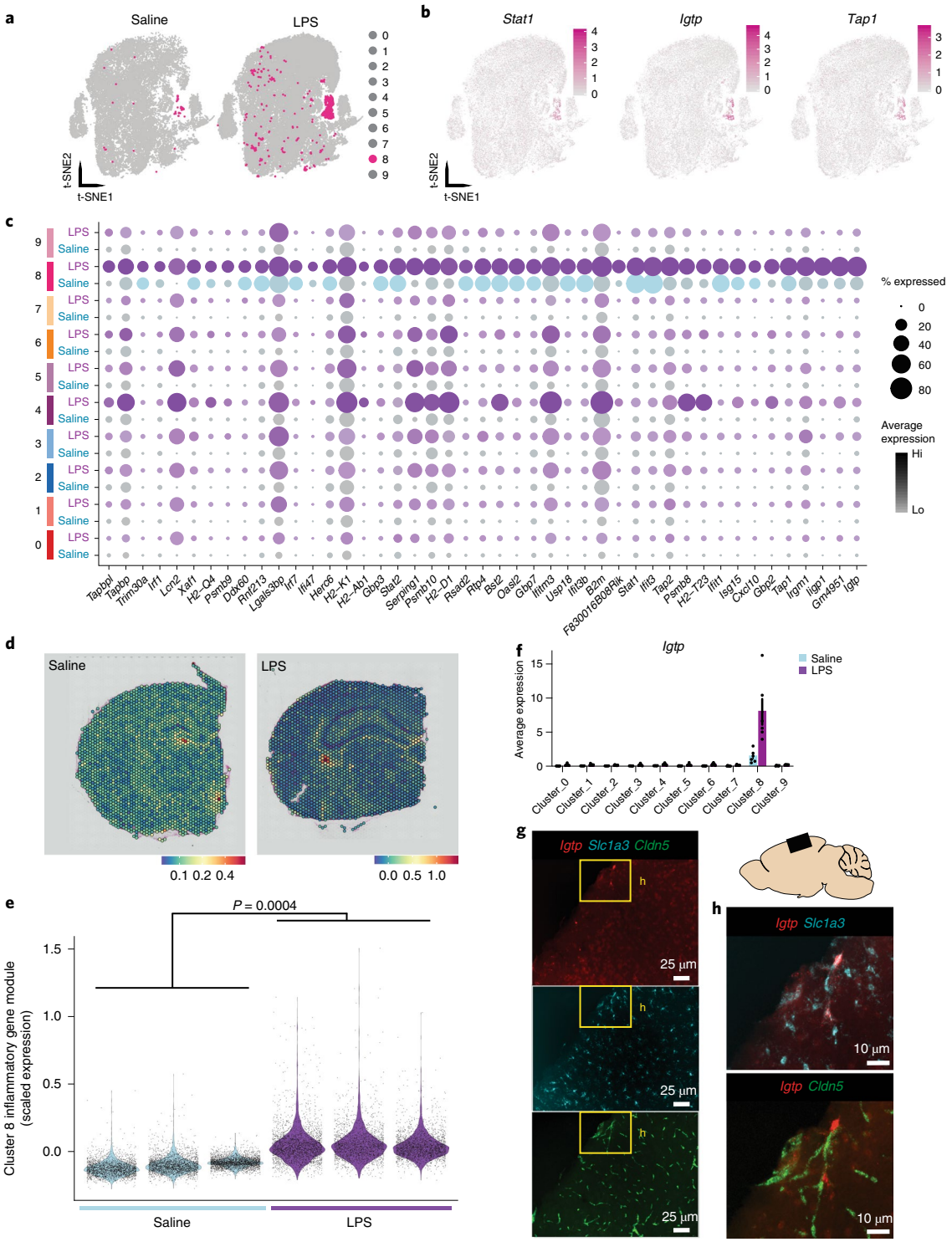

Fig. 5 | Cluster 8 is an LPS super-responder defined by interferon response genes and is closely associated with vessels, ventricles and the brain surface. a, t-SNE projection with Cluster 8 highlighted, split into saline- and LPS-injected mice. **b**, t-SNE projections highlighting example marker genes for Cluster 8, *Stat1*, *Igtp* and *Tap1* in LPS-treated animals. **c**, Dot plot showing genes enriched in Cluster 8, split into saline- and LPS-injected mice and across all clusters. Saline-injected animals are in light blue; LPS-injected animals are in purple. **d**, Visium spatial transcriptomics of Cluster 8 genes in saline- and LPS-treated animals. **e**, Quantification of Cluster 8 LPS-responsive genes in Visium brain sections from saline- and LPS-treated mice. *P* values calculated with two-tailed *t*-test on spot-averages of inflammatory gene modules. **f**, Average cluster expression of the Cluster 8 marker *Igtp* across all ten clusters split into saline and LPS. Data points represent animals—six saline- and six LPS-injected animals. Graphs show the mean; error bars are s.e.m. **g**, Inset, schematic showing location of images in **g** and **h**. **g**, RNAscope example images of Cluster 8 marker *Igtp*, astrocyte marker *Slc1a3* and blood vessel marker *Cldn5* in a brain section from an LPS-treated mouse (scale bar, 25 µm). **h**, Merged RNAscope images showing co-localization of *Igtp* with *Slc1a3* and close association of *Igtp*$^+$ astrocytes with *Cldn5*$^+$ blood vessels (scale bar, 10 µm) in Layer 1 of the cortex. Representative images from four saline- and four LPS-treated animals, but see Extended Data Fig. 7a-e for additional validation.

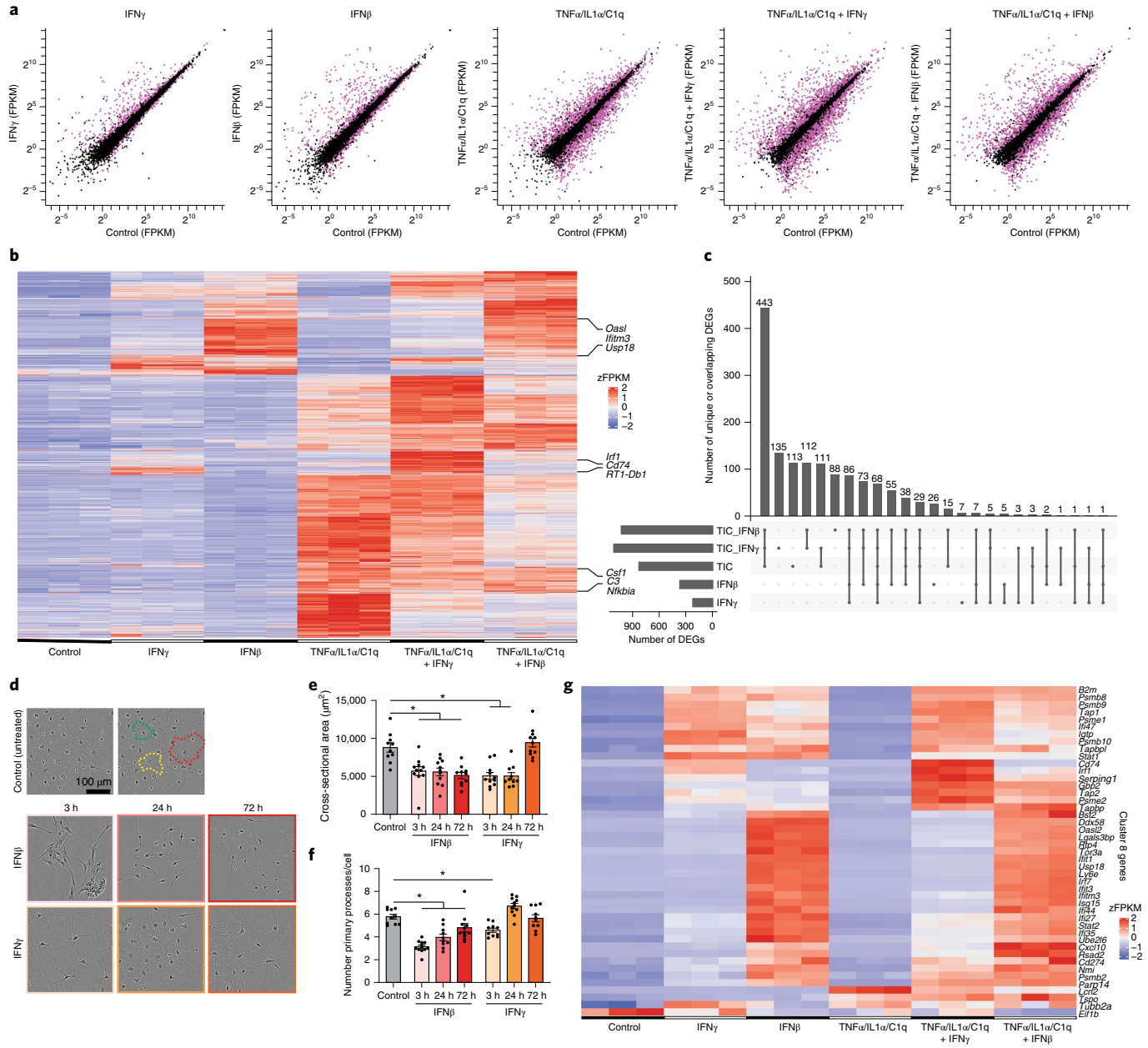

Fig. 6 | Exposure of astrocytes to interferons recapitulates the gene expression pattern of Cluster 8. a, Scatter plot of the in vitro stimulation conditions showing changes in FPKM expression in control versus 24 h after cytokine exposure to IFNγ, IFNβ, TNF/IL1α/C1q (TIC), TIC + IFNγ or TIC + IFNβ. Highlighted are genes with a $P_{adj} < 0.05$, DESeq2. **b**, Heat map showing genes that are $P_{adj} < 0.05$ in any of the five stimulation conditions, clustered by pattern of expression. Genes highlighted on the right are specific to IFNγ, IFNβ or TNF/IL1α/C1q. **c**, UpSet plot showing unique or overlapping DEGs across the cytokine stimulations. **d**, Example images of cultured astrocytes stimulated with IFNγ or IFNβ for 3 h, 24 h or 72 h. **e**, Cross-sectional area of individual astrocytes was measured from ten separate wells (50 cells measured per well). Each datapoint represents an average of 50 cells. One-way ANOVA with multiple comparisons was applied to detect significance. * represents a P value < 0.05. Bar graphs show the mean; error bars are s.e.m. **f**, Total number of primary processes radiating from individual astrocytes was counted from ten separate wells (50 cells measured per well). Each datapoint represents an average of 50 cells. One-way ANOVA with multiple comparisons was applied to detect significance. * represents a P value < 0.05. $n = 10$ replicates per group (with 50 independent measurements per replicate). Bar graphs are mean; error bars are s.e.m. **g**, Heat map showing how Cluster 8 genes are affected by addition of IFNγ, IFNβ, TIC, TIC + IFNγ or TIC + IFNβ to the culture media for 24 h.

only 142 are also induced by TIC. When comparing IFNγ to IFNβ, IFNγ has 48 uniquely induced genes, including MHC class II genes *RT1-Db2* and *RT1-DMb*, whereas IFNβ shows 195 unique genes, including the antiviral gene family *Oas1a*, *Oas2*, *Oas1k*, *Oas1f*, *Oasl* and *Oasl2*. Of the 824 TIC-induced genes, 682 are unique to TIC, including Cluster 4- and Cluster 8-enriched genes *Lcn2* and *Tspo*.

We find that both IFNγ and IFNβ can induce most Cluster 8 genes (80.0% and 91.1%, respectively), but IFNβ does so more potently (Fig. 6g). TIC on its own induces only 35.6% of Cluster 8 genes, whereas, in combination with IFNγ or IFNβ, it induces 91.1% and 95.6% of Cluster 8 genes, respectively. Indeed, IFNβ is able to induce all Cluster 8 genes except for TIC-specific genes

Lcn2 and *Tspo*, as well as *Tubb2a* and *Eif1b*, indicating that in vivo, whereas Cluster 8 is primarily induced by either IFNγ or IFNβ from a yet unknown source, it also requires the previously identified microglia-derived cytokines to attain the full Cluster 8 transcriptomic profile. This suggests a requirement of both peripheral and central activating agents for this highly specific and lowly abundant reactive astrocyte sub-state. We reported previously that exposure to TIC drastically affects astrocyte morphological complexity. To test whether exposure to interferon also affects astrocytic morphology, we added IFNγ or IFNβ to the media. Although our immunopanned astrocytes in culture exhibit a complex, process-bearing morphology in the control condition, exposure to IFNγ or IFNβ drastically changes their morphological complexity, including reduced number of primary processes and overall domain size (Fig. 6d–f). This is particularly drastic for astrocytes treated with IFNβ, which, unlike IFNγ-treated astrocytes, do not recover their normal morphology within 72 h. Together these data show that Cluster 8 reactive astrocytes are an inflammation super-responding sub-state localized to blood vessels in outer cortical layers and around the ventricles. They are induced by a combination of IFN, TNF, IL1α and C1q, suggesting a highly specialized functional role in remediation after systemic inflammation.

Interferon-responsive reactive astrocytes in disease models. Given its clear inflammatory profile, we next asked whether Cluster 8 astrocytes are present in other disease models with an inflammatory component. We integrated our scRNA-seq dataset with previously published scRNA-seq datasets from the 5XFAD mouse model of Alzheimer's disease[34,35], a mouse model of multiple sclerosis (MS) (experimental autoimmune encephalomyelitis, EAE)[36], and an acute stab wound injury model[37] (Fig. 7 and Extended Data Figs. 9 and 10). In chronic mouse models of human disease (5xFAD and EAE), no Cluster 8 astrocytes are found when analyzing the data in isolation, likely due to the low prevalence of Cluster 8 astrocytes (~2.7%) and low numbers of astrocytes sequenced in these studies. However, when integrating these smaller datasets with our larger dataset, the added power enables clustering of these small sub-states of astrocytes. In the 5xFAD mouse, we find astrocytes expressing Cluster 8 genes and their expression is partly dependent on Trem2 (Fig. 7a–c)—highlighting, again, an important interaction with immune cells in driving this response. We also find Cluster 8 astrocytes in EAE brains where it tracks the disease state being low in naive mice, highest in the acute phase and back to baseline during remission (Fig. 7d–f). Lastly, Cluster 8 astrocytes can also be found in a mouse model of a stab wound injury (Fig. 7g–i).

In this study, we made use of the power provided by high cell numbers in our scRNA-seq dataset to find small sub-states of highly reactive astrocytes that were missed in the original analyses. These integration experiments provide the enticing possibility that, although there is a heterogeneity in the astrocyte response within a single insult (for example, LPS-induced inflammation), there is some homogeneity of responses with specific sub-states of reactive astrocytes present in several conditions.

Combined, we highlight that astrocyte responses to inflammation are transcriptomically and spatially heterogeneous. These unique markers and locations highlight specific functional responses by subsets of astrocytes to the same stimulus. The transcriptomic signatures that we provide based on time, sex and anatomical location, and at the single-cell level, will allow further functional interrogation of astrocyte responses to inflammation and help to redefine how we investigate and target astrocyte activation states.

Discussion

Astrocytes play crucial homeostatic roles in the healthy brain and undergo transcriptomic and functional changes after infection and injury, as well as in chronic disease. Many of these responses can be modelled using inflammatory assays both in vitro and in vivo[6,38,39], but previous studies using a single time point or bulk sequencing have missed important information about heterogeneity of cellular responses. Here we show how heterogeneous this response is using scRNA-seq to characterize different astrocyte subset responses to inflammation and use spatial transcriptomics to highlight their anatomical location.

In a physiological setting, we show astrocytes cluster transcriptomically based on brain region, including white versus gray matter[38], and to specific cortical layers, confirming recent findings[10,11]. Additionally, although systemic inflammation causes a widespread inflammatory transition in astrocytes, this response varies among astrocyte subsets. We highlighted two clusters with particularly interesting responses to inflammation, Clusters 4 and 8, which have specific DEGs and localization in the brain.

During inflammation, Cluster 4 astrocytes expressed several potentially neuroprotective genes, including the antioxidant *Gpx1* and heat-shock protein *Hspb1*. LPS also induced the metalloproteinase inhibitor *Timp1*. Using *Timp1* RNA probes, we confirm Cluster 4 astrocytes resided in white matter tracts, suggesting they regulate extracellular matrix remodeling in white matter tracts during inflammation. In Alzheimer's disease, *Timp1* expression in astrocytes is associated with a response to amyloid β, with these astrocytes suggested to provide neuroprotection[40], possibly by block of neuronal apoptosis[41]. Astrocyte-derived TIMP1 also reportedly drives oligodendrocyte production and myelination[42]. That these *Timp1*$^{+}$ astrocytes are present in white matter tracts makes their investigation in demyelinating diseases like MS of interest as TIMP1 can promote oligodendrocyte differentiation, and *Timp1*$^{-/-}$ mice have decreased remyelination capacity[42].

Whereas Cluster 4 astrocytes exist in the healthy brain but contained key transcriptomic changes in the inflamed brain, Cluster 8 astrocytes are virtually absent in the healthy brain and are rare in the inflamed brain (2.7% of sequenced astrocytes in LPS-treated animals). Cluster 8 astrocytes express many ISGs, suggesting a gain of antigen-presenting function. Spatial transcriptomics allocates Cluster 8 to the third and lateral ventricles, the tracts connecting

Fig. 7 | Interferon-responsive astrocytes are identifiable in mouse models of disease/injury. Integration of published astrocyte datasets with the current study, to visualize IFN-responsive astrocytes. **a**, t-SNE projection of 89,420 astrocytes identified by unique astrocyte clusters (top) and original dataset (bottom). **b**, Dot plot of IFN-responsive genes. Data: 5xFAD[34] (purple), Trem2$^{-/-}$/5xFAD[35] 7-month (red), 15-month (yellow) and current study (blue). **c**, Violin plots of IFN-related transcripts split by dataset and disease. Only data from integrated Cluster 9 (that is, integrated AD and acute neuroinflammation model IFN-responsive astrocytes) are visualized. **d**, t-SNE projection of 100,471 astrocytes identified by unique astrocyte clusters (top) and original dataset (bottom). **e**, Dot plot of enriched in IFN-responsive genes. Data: EAE from two separate isolated populations[36]—one un-sorted (green) and the other *Gfap*^{TdT}-sorted (orange) and current study (blue). **f**, Violin plots of IFN-related astrocyte transcripts split by dataset and disease. Only data from integrated Cluster 10 (that is, integrated IFN-responsive astrocytes) are visualized. **g**, t-SNE projection of 83,684 astrocytes identified by unique astrocyte clusters (top) and by original dataset (bottom). **h**, Dot plot of IFN-responsive genes. Data: stab wound[37] (pink) and current study (blue). **i**, Violin plots showing IFN-related astrocyte transcripts split by dataset and disease. Only data from integrated Cluster 9 (that is, integrated IFN-responsive astrocytes) are visualized. 5X, 5xFAD; AD, Alzheimer's disease; B6, C57BL/6J mice; CFA, complete Freund's adjuvant; CNT, control; EAE, experimental autoimmune encephalomyelitis; IFN, interferon; LPS, lipopolysaccharide.

the two ventricles, and in the upper cortical layer where we find it closely associated with vessels near the surface of the brain. Furthermore, we use an in vitro approach to show that astrocytes expressing Cluster 8 DEGs can be modelled using IFNβ. By integrating scRNA-seq datasets, we confirmed Cluster 8 astrocytes in a range of disease models, namely Alzheimer's disease, EAE and acute

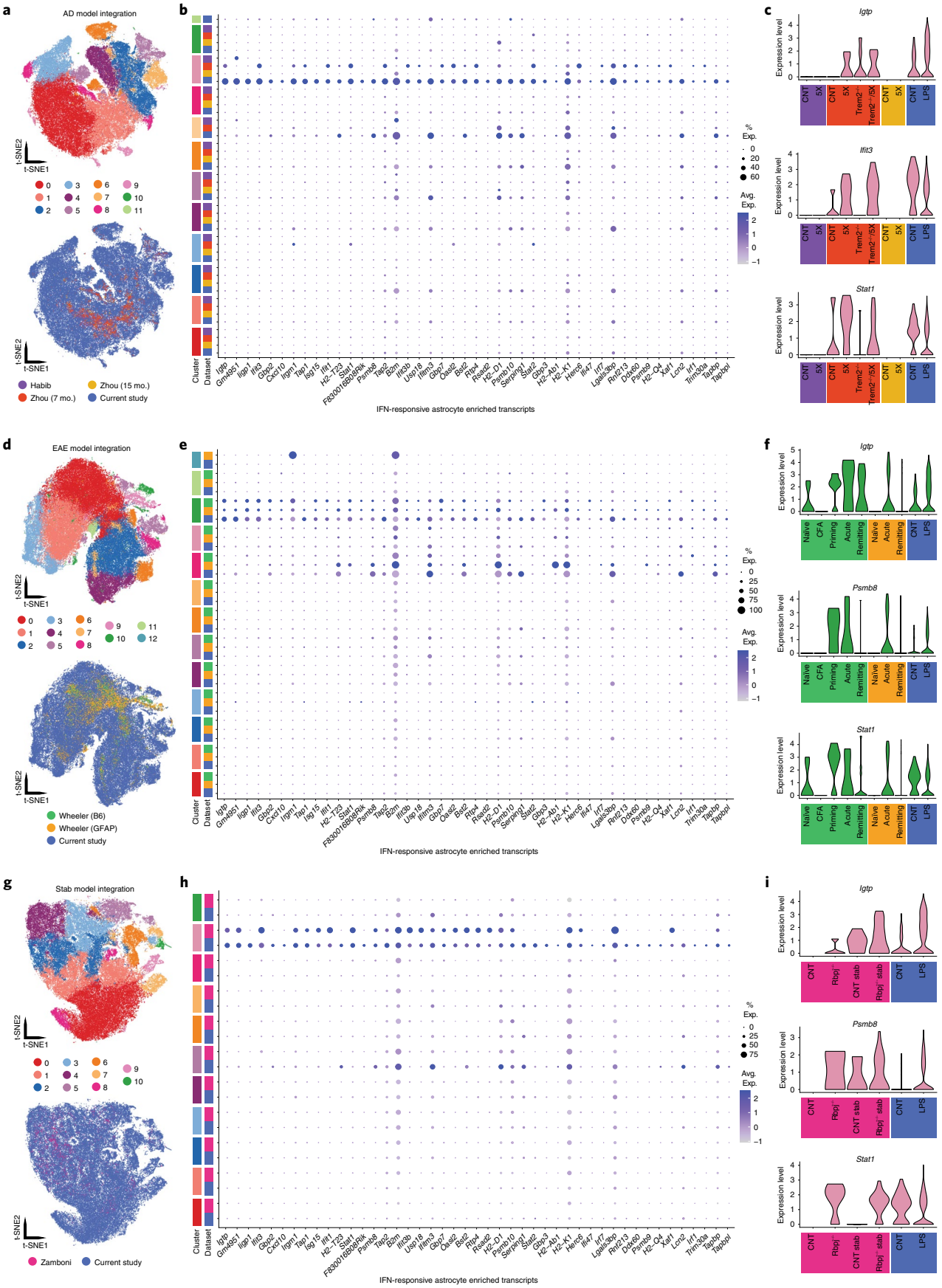

stab wound. Cluster 8 astrocytes are also defined by high levels of the chemokine *Cxcl10*. *Cxcl10*$^+$ astrocytes surrounding vessels are reported in patients with MS[43], and their location could make it a powerful astrocytic subtype to target therapeutically. Furthermore, STAT1-IGTP signaling is implicated as a key mediator of interferon signaling required for astrocytes to respond to *Toxplasma gondii* infection[44,45], and we hypothesize that Cluster 8 astrocytes serve as gatekeepers from peripheral insults.

It is not clear what informs this differential change in inflammatory gene signatures across clusters. It is possible that groups of astrocytes show different competences (for example, cytokine receptor expression) and, therefore, respond differently to common stimuli. Alternatively, different regions of the brain might be affected in different ways by an inflammatory insult like LPS. We find that both Cluster 4 and Cluster 8 astrocytes are located at strategic locations: closely associated with ventricles, blood vessels or subpial areas—regions where peripheral immune cells are more readily able to interact with the CNS. Indeed, Cluster 8 astrocyte location and interferon response signature indicate that infiltrating leukocytes likely induce this gene signature.

We want to also note limitations of this study. First, LPS, as an inducer of brain inflammation, creates a response in astrocytes but might induce inflammatory responses dissimilar to subtle inflammation present in chronic neurodegenerative disease. Although we cannot completely rule this out, we confirm Cluster 8 signatures in several acute and chronic disease mouse models. Second, we only study here the acute (3–72 h) response of astrocytes to inflammation. In chronic diseases, such as Alzheimer's disease, years of inflammation likely create complex astrocyte reactivity states induced and modified by a myriad of factors. Although we confirm Cluster 8 astrocytes in mouse models of Alzheimer's disease and MS, future work should apply the multimodal tools that we used here on other diseases, particularly on human tissue. Third, our scRNA-seq dataset was generated from astrocytes purified from cortex and underlying white matter, but we highlight our clusters throughout several other brain areas. Thus, we can only be sure that the signal we see in cortex (including subpial regions) as well as white matter (particularly corpus callosum) are truly created by the clusters we identified, and that the subcortical signal (for example, *Myoc*$^+$ astrocytes below the hippocampus or astrocytes in the SVZ) could be subsets that express additional genes beyond those reported here. Finally, although we identified markers for both Cluster 8 (*Igtp*) and Cluster 4 (*Timp1*), these genes are also induced by LPS in other clusters, albeit minimally. As a result, using these markers to confirm absence or presence of either cluster has to be performed contextually. For example, a Cluster 4 astrocyte can only be identified by its strong (inflammation-induced) expression of *Timp1* and its position within white matter tracts.

Combined, these data show that astrocytes produce spatial, temporal, sex-specific and subtype-specific responses to inflammation and should enable functional interrogation of individual subsets going forward. These data also present a comprehensive set of DEGs for development of new visualization tools to track individual subsets of reactive astrocytes during disease. We also provide these data as a baseline for incorporation of sequencing datasets from other brain regions. Many important questions can now be addressed. Is regional heterogeneity maintained during responses to chronic infection and disease? Are there species-specific astrocyte inflammatory pathways? We hope that integration of our data with future scRNA-seq efforts will address these questions.

Online content

Any methods, additional references, Nature Research reporting summaries, source data, extended data, supplementary information, acknowledgements, peer review information; details of author contributions and competing interests; and statements of data and code availability are available at https://doi.org/10.1038/s41593-021-00905-6.

Received: 14 April 2020; Accepted: 8 July 2021;
Published online: 19 August 2021

References

1. Nedergaard, M., Ransom, B. & Goldman, S. A. New roles for astrocytes: redefining the functional architecture of the brain. *Trends Neurosci.* **26**, 523–530 (2003).
2. Magistretti, P. J. & Allaman, I. Lactate in the brain: from metabolic end-product to signalling molecule. *Nat. Rev. Neurosci.* **19**, 235–249 (2018).
3. Alvarez, J. I., Katayama, T. & Prat, A. Glial influence on the blood brain barrier. *Glia* **61**, 1939–1958 (2013).
4. Zamanian, J. L. et al. Genomic analysis of reactive astrogliosis. *J. Neurosci.* **32**, 6391–6410 (2012).
5. Karimi-Abdolrezaee, S. & Billakanti, R. Reactive astrogliosis after spinal cord injury-beneficial and detrimental effects. *Mol. Neurobiol.* **46**, 251–264 (2012).
6. Liddelow, S. A. et al. Neurotoxic reactive astrocytes are induced by activated microglia. *Nature* **541**, 481–487 (2017).
7. Liddelow, S. A. & Barres, B. A. Reactive astrocytes: production, function, and therapeutic potential. *Immunity* **46**, 957–967 (2017).
8. Clarke, L. E. et al. Normal aging induces A1-like astrocyte reactivity. *Proc. Natl Acad. Sci. USA* **115**, E1896–E1905 (2018).
9. Chai, H. et al. Neural circuit-specialized astrocytes: transcriptomic, proteomic, morphological, and functional evidence. *Neuron* **95**, 531–549.e9 (2017).
10. Bayraktar, O. A. et al. Astrocyte layers in the mammalian cerebral cortex revealed by a single-cell in situ transcriptomic map. *Nat. Neurosci.* **23**, 500–509 (2020).
11. Batiuk, M. Y. et al. Identification of region-specific astrocyte subtypes at single cell resolution. *Nat. Commun.* **11**, 1–15 (2020).
12. Zeisel, A. et al. Cell types in the mouse cortex and hippocampus revealed by single-cell RNA-seq. *Science* **347**, 1138–1142 (2015).
13. Zeisel, A. et al. Molecular architecture of the mouse nervous system. *Cell* **174**, 999–1014 (2018).
14. Saunders, A. et al. Molecular diversity and specializations among the cells of the adult mouse brain. *Cell* **174**, 1015–1030 (2018).
15. Hasel, P. et al. Neurons and neuronal activity control gene expression in astrocytes to regulate their development and metabolism. *Nat. Commun.* **8**, 15132 (2017).
16. Buttini, M. & Boddeke, H. Peripheral lipopolysaccharide stimulation induces interleukin-1β messenger RNA in rat brain microglial cells. *Neuroscience* **65**, 523–530 (1995).
17. Spencer, J. A. et al. Altered vascular remodeling in fibulin-5-deficient mice reveals a role of fibulin-5 in smooth muscle cell proliferation and migration. *Proc. Natl Acad. Sci. USA* **102**, 2946–2951 (2005).
18. Zhou, Y. et al. Metascape provides a biologist-oriented resource for the analysis of systems-level datasets. *Nat. Commun.* **10**, 1523 (2019).
19. Pinheiro, I. et al. LPS resistance of SPRET/Ei mice is mediated by Gilz, encoded by the *Tsc22d3* gene on the X chromosome. *EMBO Mol. Med.* **5**, 456–470 (2013).
20. Ronchetti, S., Migliorati, G. & Riccardi, C. GILZ as a mediator of the anti-inflammatory effects of glucocorticoids. *Front. Endocrinol. (Lausanne)* **6**, 170 (2015).
21. Butler, A., Hoffman, P., Smibert, P., Papalexi, E. & Satija, R. Integrating single-cell transcriptomic data across different conditions, technologies, and species. *Nat. Biotechnol.* **36**, 411–420 (2018).
22. Stuart, T. et al. Comprehensive integration of single-cell data. *Cell* **177**, 1888–1902 (2019).
23. Crowell, H. L. et al. Muscat detects subpopulation-specific state transitions from multi-sample multi-condition single-cell transcriptomics data. *Nat. Commun.* **11**, 1–12 (2020).
24. Mizrak, D. et al. Single-cell analysis of regional differences in adult V-SVZ neural stem cell lineages. *Cell Rep.* **26**, 394–406 (2019).
25. Christopherson, K. S. et al. Thrombospondins are astrocyte-secreted proteins that promote CNS synaptogenesis. *Cell* **120**, 421–433 (2005).
26. Kucukdereli, H. et al. Control of excitatory CNS synaptogenesis by astrocyte-secreted proteins Hevin and SPARC. *Proc. Natl Acad. Sci. USA* **108**, E440–E449 (2011).
27. Bar, O., Gelb, S., Atamny, K., Anzi, S. & Ben-Zvi, A. Angiomodulin (IGFBP7) is a cerebral specific angiocrine factor, but is probably not a blood–brain barrier inducer. *Fluids Barriers CNS* **17**, 1–13 (2020).
28. Lin, M. et al. Cell surface antigen CD109 is a novel member of the α_2 macroglobulin/C3, C4, C5 family of thioester-containing proteins. *Blood* **99**, 1683–1691 (2002).

29. Bizet, A. A. et al. The TGF-β co-receptor, CD109, promotes internalization and degradation of TGF-β receptors. *Biochim. Biophys. Acta* **1813**, 742–753 (2011).
30. Hung, C. C. et al. Astrocytic GAP43 induced by the TLR4/NF-κB/STAT3 axis attenuates astrogliosis-mediated microglial activation and neurotoxicity. *J. Neurosci.* **36**, 2027–2043 (2016).
31. Song, W., Li, D., Tao, L., Luo, Q. & Chen, L. Solute carrier transporters: the metabolic gatekeepers of immune cells. *Acta Pharm. Sin. B* **10**, 61–78 (2020).
32. Furukawa, J. et al. Functional identification of SLC43A3 as an equilibrative nucleobase transporter involved in purine salvage in mammals. *Sci. Rep.* **5**, 1–11 (2015).
33. Foo, L. C. et al. Development of a method for the purification and culture of rodent astrocytes. *Neuron* **71**, 799–811 (2011).
34. Habib, N. et al. Disease-associated astrocytes in Alzheimer's disease and aging. *Nat. Neurosci.* **23**, 701–706 (2020).
35. Zhou, Y. et al. Human and mouse single-nucleus transcriptomics reveal TREM2-dependent and TREM2-independent cellular responses in Alzheimer's disease. *Nat. Med.* **26**, 131–142 (2020).
36. Wheeler, M. A. et al. MAFG-driven astrocytes promote CNS inflammation. *Nature* **578**, 593–599 (2020).
37. Zamboni, M., Llorens-Bobadilla, E., Magnusson, J. P. & Frisén, J. A widespread neurogenic potential of neocortical astrocytes is induced by injury. *Cell Stem Cell* **27**, 605–617 (2020).
38. Cahoy, J. D. et al. A transcriptome database for astrocytes, neurons, and oligodendrocytes: a new resource for understanding brain development and function. *J. Neurosci.* **28**, 264–278 (2008).
39. Hamby, M. E. et al. Inflammatory mediators alter the astrocyte transcriptome and calcium signaling elicited by multiple G-protein-coupled receptors. *J. Neurosci.* **32**, 14489–14510 (2012).
40. Saha, P., Sarkar, S., Paidi, R. K. & Biswas, S. C. TIMP-1: a key cytokine released from activated astrocytes protects neurons and ameliorates cognitive behaviours in a rodent model of Alzheimer's disease. *Brain. Behav. Immun.* **87**, 804–819 (2020).
41. Ashutosh, C. Chao, Borgmann, K., Brew, K. & Ghorpade, A. Tissue inhibitor of metalloproteinases-1 protects human neurons from staurosporine and HIV-1-induced apoptosis: mechanisms and relevance to HIV-1-associated dementia. *Cell Death Dis.* **3**, e332–e339 (2012).
42. Moore, C. S. et al. Astrocytic tissue inhibitor of metalloproteinase-1 (TIMP-1) promotes oligodendrocyte differentiation and enhances CNS myelination. *J. Neurosci.* **31**, 6247–6254 (2011).
43. Sørensen, T. L. et al. Expression of specific chemokines and chemokine receptors in the central nervous system of multiple sclerosis patients. *J. Clin. Invest.* **103**, 807–815 (1999).
44. Halonen, S. K., Taylor, G. A. & Weiss, L. M. Gamma interferon-induced inhibition of *Toxoplasma gondii* in astrocytes is mediated by IGTP. *Infect. Immun.* **69**, 5573–5576 (2001).
45. Hidano, S. et al. STAT1 signaling in astrocytes is essential for control of infection in the central nervous system. *MBio* **7**, 1–15 (2016).

Methods

Animals. P30–35 '*Aldh1l1*^{eGFP}' (Tg(Aldh1l1-EGFP)OFC789Gsat/Mmucd, RRID:MMRRC_011015-UCD)[46] mice were used in most experiments. Mice were housed on a 12-h light/dark cycle and had food and water ad libitum. All animal procedures were in accordance with the guidelines provided by the National Institute of Health as well as NYU Langone School of Medicine's Administrative Panel on Laboratory Animal Care. All animals were housed at 22–25 °C and 50–60% humidity.

LPS injections. Male and female mice were weighed and injected intraperitoneally with either 5 mg kg^{-1} of LPS (55:B5 Sigma-Aldrich, L2880) or physiological endotoxin-free saline (Enzo Life Sciences, alx-505-009-Id15) using one insulin syringe (BD, 328418) per animal, and tissue was harvested after 3 h, 24 h or 72 h for downstream analysis.

Cell Isolation. Animals were euthanized using CO_2, and brains were immediately put into PBS for dissection. Cortices were removed from the rest of the brain, diced into 1-mm^3 cubes and moved into enzyme solution (1× EBSS (Sigma-Aldrich, E7510), 0.46% glucose (VWR, AAA16828- 0E), 26 mM $NaHCO_3$ (Sigma-Aldrich, S4019), 0.5 mM EDTA (Sigma-Aldrich, 27285)) containing 200 U of papain per brain (Worthington Biochemical, LS003126) and incubated for 40 min at 37 °C with the tissue being agitated every 10 min. All solutions used throughout contained 125 Units DNAse ml^{-1} (Worthington Biochemical, LS002007). The brain tissue was then transferred into a canonical tube and, after it settled, was washed three times with a trypsin inhibitor solution (1× EBSS (Sigma-Aldrich, E7510), 0.46% glucose (VWR, AAA16828- 0E), 26 mM $NaHCO_3$ (Sigma-Aldrich, S4019)) in the presence of 1× low-ovomucoid solution (10× stock: 15 mg ml^{-1} of BSA (Sigma-Aldrich, A4161) and 15 mg ml^{-1} of ovomucoid (Worthington Biochemical, LS003086)). All following steps were performed either on wet ice or at 4 °C. After the last wash, cells were carefully triturated using a 2-ml serological pipette, letting non-homogenized tissue settle, and repeated twice more until most tissue was dissociated. The cells were transferred into a new canonical tube and a high ovomucoid solution (1× EBSS (Sigma-Aldrich, E7510), 0.46% glucose (VWR, AAA16828-0E), 26 mM $NaHCO_3$ (Sigma-Aldrich, S4019)) in the presence of 1× Hi-ovomucoid solution (10× stock: 30 mg ml^{-1} of BSA (Sigma-Aldrich, A4161), 30 mg ml^{-1} of ovomucoid (Worthington Biochemical, LS003086)) and was carefully pipetted to the bottom of the tube. Cells were centrifuged at 400*g* for 5 min at 4 °C, and the pellet was resuspended in 10 ml of PBS (Invitrogen, 14190144). The cell suspension was then passed through a Nitex mesh filter (Nitex, 20 µM Tetko HC3-20) and then spun at 400*g* for 5 min and resuspended in 500 µl of PBS containing 1% BSA.

FACS. All cell sorting experiments were performed on a Sony SH800Z with a 100-µm nozzle at 4 °C. P30–35 '*Aldh1l1*^{eGFP}' mice were used for sorting, and gates were set to collect single cells that were DAPI (Thermo Fisher Scientific, D1306) negative and GFP positive (Extended Data Fig. 1). About 100,000 astrocytes were collected for each sample into PBS containing 1% BSA.

RNA extraction. For bulk RNA-seq, RNA was extracted using the Absolutely Total RNA Purification Kit (Agilent), following the manufacturer's instructions. FACS-purified astrocytes were spun down at 400*g* for 5 min at 4 °C and resuspended in the supplied lysis buffer. The RNA extraction included a DNAse incubation step, and RNA was eluted in 11 µl of RNAse-free water. RNA integrity was assessed using the Agilent Bioanalyzer.

10x single-cell pipeline. After FACS purification, astrocytes were counted on a hemocytometer, spun down at 400*g* for 5 min at 4 °C and resuspended in PBS containing 0.4% BSA to 600–1,600 cells per µl. Cells were then prepared using the 10x Chromium Single Cell Gene Expression kit (V2) according to the manufacturer's instruction using the V2 chemistry. Next, 17,400 cells per condition were loaded onto the Single Cell A Chip with the goal to recover 10,000 cells per sample. Gel bead-in emulsions were created using the Chromium Controller, followed by cDNA synthesis, amplification and library construction following the 10x pipeline.

Library prep and RNA sequencing. For RNA from in vitro and in vivo bulk astrocytes, cDNA was generated using the SMART-seq HT kit, and libraries were generated using the Nextera XT kit (Takara Bio). All libraries were sequenced on an Illumina NovaSeq 6000. The 12 single-cell libraries were run on an S2 100 flow cell at the NYU School of Medicine Genome Technology Center. After sequencing, data were prepared as follows: Illumina NovaSeq 6000 RTA (v3.4.4) software was used to perform basecalling, and per-read, per-sample FASTQ files were generated using the bcl2fastq Conversion software (v2.20) to convert BCL base call files outputted by the sequencing instrument into the FASTQ format.

Bulk RNA-seq analysis. FASTQ files for each sample were concatenated and groomed using FASTQ Groomer[47], aligned to the mm10 reference genome using HISAT2 (v.2.1.0)[48] followed by transcript assembly and quantification using StringTie (v2.1.1)[49]. Differential gene expression was assessed using DESeq2 (v2.11.40.6)[50]. Expression values are given as FPKM (fragments per kilobase millions). Heat maps were generated using the R package ComplexHeatmap (v2.1.0)[51]. GO term analysis was performed using Metascape's multiple gene list function[18], and additional data visualization was performed with Prism8 (v8.2.1), *circlize* (v2.1.0), *VennDiagram* (v1.6.20), *ggplot2* (v3.2.1) and *upSetR* (v1.4.0). Some of the bulk RNA-seq analysis was also performed in Microsoft Excel (v16.14.1).

Single-cell RNA-seq data analysis. The 10x Genomics single-cell RNA-seq analysis software Cell Ranger (v3.0.2), specifically the 'cellranger count' pipeline, was used to align reads from the generated FASTQ files to the mouse reference genome mm10 and to generate gene–barcode expression matrices. The outputs of the 12 samples from the 'cellranger count' pipeline were aggregated using the 'cellranger aggr' pipeline of Cell Ranger, normalizing the combined output to the same sequencing depth and recomputing the gene–barcode matrices and expression analysis accordingly for the aggregated data.

Further single-cell RNA-seq analysis was performed following the *muscat* (v.0.99.9) R package pipeline[23], which facilitates multi-sample, multi-condition comparisons of single-cell RNA-seq data. After doublet detection using *scds* (v1.1.2) and calculation of the mitochondrial gene contribution using *scater* (v1.13.23) within the SingleCellExperiment library (v1.7.11), cells were filtered using the median absolute deviation (MAD) module where cells containing a greater than 2.5 MAD in feature counts, number of expressed features and percentage of mitochondrial genes were discarded. Subsequently, only genes with count numbers higher than 1 in more than 20 cells were retained (Extended Data Figs. 3 and 10). Using *seurat* (v3.1.0)[21,22], data were log normalized, and the 2,000 most variable features were identified for each sample separately. Using 30 dimensions, the samples were anchored and integrated using canonical correlation analysis to find common cell populations. This was followed by scaling and linear dimensional reduction using principal component analysis (PCA) of the variable features and non-linear dimensional reduction in the form of a t-distributed stochastic neighbor embedding (t-SNE) using 20 principal components. Using a 0.1 resolution, we identified clear clusters that were subsequently identified by querying sets of known cell type marker genes (Extended Data Fig. 1b). About 8% of all cells were non-astrocytic (namely, neurons, oligodendrocytes, oligodendrocyte precursor cells, endothelial cells, pericytes, blood cells and microglia) and were removed from the dataset using *seurat*'s subset function, leaving approximately 80,000 astrocytes for downstream analysis. In the second iteration of clustering in which only astrocytes were evaluated, we identified a new set of 2,000 variable features for each sample and followed the same pipeline as described above. We then calculated DEGs between conditions using *edgeR* (v3.27.13) on the sum of counts across all samples of each condition for each cluster as described in the *muscat* pipeline, using false discovery rate < 0.05 as cutoff. Tools within the *muscat* DEG pipeline also included *dplyr* (v0.8.3), *purr* (v0.3.3) and *scran* (v1.13.25). For scRNA-seq data visualization, we employed *LSD* (v4.0-0), *CATALYST* (v1.9.8), *RColorBrewer* (v1.1-2), *viridis* (v0.5.1) and *seurat* (v3.1.0).

For scRNA-seq dataset integration analyses, we obtained Cell Ranger files for each published dataset and followed the same quality control (QC), normalization, anchoring and integration procedures as listed above. Once only astrocyte populations were identified in each dataset, we merged all astrocyte-specific objects and repeated the normalization, anchoring and integration process to created multi-dataset objects comparing our acute inflammation model with Alzheimer's disease models, an MS model and a stab wound injury model, respectively. Code for this integration and scRNA-seq reanalysis can be obtained via the following GitHub Repository: https://github.com/liddelowlab/Hasel_et_al.

Visium spatial transcriptomic. Brains from saline- and LPS-injected P30 *Aldh1l1*^{eGFP} mice were harvested 24 h after injection and frozen down in OCT on dry ice. Brains were sectioned coronally to 10 µm on a cryostat and mounted on the Visium Spatial Gene Expression Slide. All sections had a RNA integrity number > 8 as measured using a Bioanalyzer (Agilent). Sections were methanol fixed at −20 °C for 30 min and stained for hematoxylin and eosin for general morphological analyses and spatial alignment of sequencing data. After bright-field imaging, brain sections were enzymatically permeabilized for 12 min, poly-A mRNA captured on each of the spots on the capture area and spatial barcodes and unique molecular identifiers were added to the reads. The eight dual-index Illumina paired-end libraries were sequenced on a NovaSeq 6000 on an S2 100-cycle flow cell, and the RNA-seq output was aligned to the mouse reference genome mm10 and images detected using SpaceRanger (v1.2.0). Data were analyzed using *seurat* (v3.1.0). In short, each section was normalized using SCTransform and merged based on variable features. To highlight clusters identified in our single-cell RNA-seq data, we selected genes differentially expressed ≥ natural log 0.35 using the AddModuleScore function in *seurat*.

NanoString. NanoString nCounter technology was used to measure expression analysis of 770 genes associated with glia and reactive astrocyte subtypes (NanoString, XT-CSO-M GLIAL-12) from samples previously used for single-cell and RNAscope experiments. Three to five 150-µm sagittal sections were cut from fresh-frozen brains (see above) and total RNA extracted using QIAshredder and

Qiagen RNeasy columns. RNA samples were measured using a NanoDrop, and only those with a concentration above 20.0 ng μl^{-1} were used for downstream analysis (100 ng total RNA run for each sample). The nCounter Glial Profiling Panel (NanoString) was run on an nCounter according to supplier protocols by the Gene Technology Center at NYU School of Medicine. Analysis of raw data was completed using the ROSALIND online platform from OnRamp (https://rosalind.onramp.bio/), with a HyperScale architecture developed by OnRamp BioInformatics. Read distribution percentages, identity heat maps and sample multi-dimensional scaling plots were generated as part of the QC step. Samples used for analysis had the following QC metrics: %FOV captured: 99.75 ± 0.09, binding density: 2.11 ± 0.16, positive control linearity: 1.00 ± 3.54 × 10^{-5} and noise threshold: 4.84 ± 0.36. Normalization was completed by dividing counts within a lane by the geometric mean of the normalizer probes from the same lane. The NormqPCR R library[52] was then used to select normalizer probes using the geNorm algorithm. Fold changes and *P* values were calculated using criteria provided by NanoString. Clustering of genes for the final heat map of DEGs was done using the PAM (Partitioning Around Medoids) method using the fpc R library that takes into consideration the direction and type of all signals on a pathway, the position, role and type of every gene.

Cell culture and in vitro interferon experiments. Astrocytes were purified by immunopanning from P5 Sprague Dawley rat pups (Charles River, Strain Code 400) as previously described[33]. Briefly, cortices were dissected and enzymatically digested for 40 min at 34 °C in 22 ml of a 0.2-µm syringe-filtered enzyme solution consisting of sterile H_2O, 1× EBSS (Sigma-Aldrich, E7510), 0.36% D(+)-glucose, 26 mM $NaHCO_3$, 0.5 mM EDTA, 0.004 g of L-cysteine (Sigma-Aldrich, C7880) and 100 U of papain (Worthington Biochemical, LS003126). A 5% CO_2/95% O_2 gas mixture was used to maintain the pH of the papain solution during the dissociation.

Cortices were then mechanically dissociated in 1× EBSS, 0.36% D(+)-glucose, 26 mM $NaHCO_3$, 0.002% DNase (Worthington Biochemical, LS002007), 0.10% ovomucoid trypsin inhibitor (Worthington Biochemical, LS003086) and 0.10% BSA (Sigma-Aldrich, A8806). The resultant single-cell supernatant was collected, and an ovomucoid density gradient was made by layering a high ovomucoid solution (sterile H_2O containing 1× EBSS, 0.36% D(+)-glucose, 26 mM $NaHCO_3$, 0.001% DNase, 0.50% ovomucoid and 0.50% BSA) below the single-cell suspension. After spinning at 110 r.c.f. for 5 min, the cell pellet was resuspended in 9 ml of 0.02% BSA/DNase in D-PBS (HyClone, SH30264.01), filtered through a 0.22-µm nitex mesh filter (Tetko HC3-20) and incubated for 40 min at 37 °C to allow return of antigens to the cell surface.

After incubation, the single-cell solution was passed through panning plates to deplete non-astrocytic cell types before astrocytes were positively selected by a 40-min incubation on an anti-ITGB5 (eBioscience, 14-0497) plate. After removal of unbound single-cell suspension and washing with D-PBS, 200 U trypsin (Sigma-Aldrich, T9201) in 1× EBSS without Mg^{2+} or Ca^{2+} (Sigma-Aldrich, E6267) was added to the anti-ITGB5 plate and then incubated for 3 min in a 37 °C/10% CO_2 incubator. Astrocytes were dislodged using 20 ml of 30% FBS (Seradigm, 1500-500H) in a 1:1 mixture of neurobasal (Gibco, 21103) and DMEM (Gibco 11960-044). After addition of 100 µl of 0.4% DNase per 10 ml of suspended cells, dislodged cells were centrifuged at 170 r.c.f. for 11 min. After removal of supernatant, the cell pellet was resuspended in astrocyte base media consisting of 50% neurobasal, 50% DMEM, penicillin–streptomycin (100 U ml^{-1} of penicillin; 100 µg ml^{-1} of streptomycin, Gibco 15140-122), sodium pyruvate (1 mM, Gibco, 11360-070), L-glutamine (292 µg ml^{-1}, Gibco, 25030-081), 1× neurobasal-based SATO supplement and *N*-acetyl cysteine (5 µg ml^{-1}, Sigma-Aldrich, A8199). Astrocytes were plated on tissue culture plates coated with poly-D-lysine (Sigma-Aldrich, P6407, prepared in sterile H_2O) at a density of 50,000 per well in six-well plates. Astrocytes were left to recover in astrocyte base media supplemented with HBEGF (5 ng ml^{-1}, Sigma-Aldrich, E4643) in a 37 °C/10% CO_2 incubator.

Six days after plating, isolated astrocytes were given a half medium change with fresh 5 ng ml^{-1} HBEGF and with either IFNγ (3 ng ml^{-1}, abcam ab198568) or IFNβ (1,000 U ml^{-1}, Sigma-Aldrich, I8907) for 3, 24 and 72 h. At these time points, treated astrocytes were phase imaged (Incucyte S3 System) using a ×10 objective lens. The size and morphological complexity of purified and cultured rat astrocytes treated with interferons and previously described activators of neuroinflammatory reactive astrocytes (IL1α, TNF and C1q) were measured in Fiji. For the cross-sectional area, the polygon selection tool was used to connect the maximum point from the cell body of each process and the measure function used to provide the area in μm^2. Process numbers were counted by eye. A minimum of 20 astrocytes from five random regions of interest from six separate image areas were counted across at least ten separate cell culture wells per treatment. Cell area and process number are averaged per well and plotted as individual values per well.

A separate set of astrocytes were treated with IFNγ (3 ng ml^{-1}, abcam, ab198568), IFNβ (1,000 U ml^{-1}, Sigma-Aldrich, I8907), the previously reported neuroinflammatory reactive astrocyte activating cocktail of IL1α (3 ng ml^{-1}, Sigma-Aldrich, I3901), TNF (30 ng ml^{-1}, Cell Signaling Technology, 8902SF) and C1q (400 ng ml^{-1}, MyBioSource, MBS143105) or combinations of IFNγ + IL1α + TNF + C1q or IFNβ + IL1α + TNF + C1q using the same concentrations. At 24 h after cytokine stimulation, RNA was extracted using the Absolutely Total RNA Purification Kit (Agilent), following the manufacturer's instructions, and data were processed as described above.

In situ hybridization. RNA in situ hybridization was performed using the RNAscope Fluorescent Multiplex Assay (ACD). Un-perfused brains were washed in PBS and frozen in OCT (Sakura, 4583). Brains were sectioned on a cryostat at 20 µm and mounted on slides. As per the protocol provided by the manufacturer, brain sections were fixed in 4% paraformaldehyde at 4 °C for 15 min, ethanol-dehydrated and protease-permeabilized. Brain sections were then incubated for 2 h with the probes at 40 °C followed by several rounds of signal amplification before mounting in Fluoromount-G mounting medium (Southern Biotech, 0100-01). Images were taken using a fluorescent microscope (Keyence BZ-X710) and processed in Fiji[53]. Probes used were as follows: *Igtp*-C1: 816881, *Slc1a3*-C3:430781, *Cldn5*-C2: 491611, *Timp1*-C1: 316841. For quantification, cells were deemed *Igtp*$^+$ or *Timp1*$^+$ when 20 or more dots were counted per cell and co-localized with *Slc1a3*. Two to three sections from four saline- and four LPS-treated animals were used for quantification. *Igtp*$^+$ cells were counted in Layer1, and *Timp1*$^+$ cells were counted in the corpus callosum.

Statistics and reproducibility. Sample sizes were determined based on previous publications, and independent biological replicates range from 3 to 6 for all experimental modalities used in this study. All statistical tests used are highlighted in the legend of each figure. No data were excluded from the analyses. The experiments were not randomized. The investigators were not blinded to allocation during experiments and outcome assessment.

Reporting Summary. Further information on research design is available in the Nature Research Reporting Summary linked to this article.

Data availability

All sequencing data generated in association with this study are available in the Gene Expression Omnibus as a SuperSeries under accession number GSE148612. Mouse scRNA-seq is available under accession number GSE148611, mouse bulk RNA-seq is available under accession number GSE148610, mouse spatial transcriptomic under GSE165098 and rat bulk RNA-seq data are available under accession number GSE165069. Bulk sequencing of in vivo mouse astrocytes, in vivo mouse astrocyte scRNAseq pseudobulk and in vitro rat astrocyte bulk RNA-seq are available to search on www.gliaseq.com. scRNA-seq at single-cell resolution as well as spatial transcriptomic data are available on www.gliaseqpro.com. NanoString data are available on https://rosalind.onramp.bio/showcase/liddelow.
scRNA-seq data from other studies referenced in Fig. 7 and Extended Data Figs. 9 and 10 are available from the Gene Expression Omnibus under accession numbers GSE143758, GSE140511, GSE130119 and GSE139842.
Details of analysis pipeline libraries are listed in Methods and available at https://github.com/liddelowlab/Hasel_et_al.

References

46. Gong, S. et al. A gene expression atlas of the central nervous system based on bacterial artificial chromosomes. *Nature* **425**, 917–925 (2003).
47. Blankenberg, D. et al. Manipulation of FASTQ data with galaxy. *Bioinformatics* **26**, 1783–1785 (2010).
48. Kim, D., Langmead, B. & Salzberg, S. L. HISAT: a fast spliced aligner with low memory requirements. *Nat. Methods* **12**, 357–360 (2015).
49. Pertea, M. et al. StringTie enables improved reconstruction of a transcriptome from RNA-seq reads. *Nat. Biotechnol.* **33**, 290–295 (2015).
50. Love, M. I., Huber, W. & Anders, S. Moderated estimation of fold change and dispersion for RNA-seq data with DESeq2. *Genome Biol.* **15**, 1–21 (2014).
51. Gu, Z., Eils, R. & Schlesner, M. Complex heatmaps reveal patterns and correlations in multidimensional genomic data. *Bioinformatics* **32**, 2847–2849 (2016).
52. Perkins, J. R. et al. ReadqPCR and NormqPCR: R packages for the reading, quality checking and normalisation of RT–qPCR quantification cycle (Cq) data. *BMC Genomics* **13**, 296 (2012).
53. Schindelin, J. et al. Fiji: an open-source platform for biological-image analysis. *Nat. Methods* **9**, 676–682 (2012).

Acknowledgements

We thank all members of the Liddelow lab at NYU Grossman School of Medicine for support and advice and K. Guttenplan for careful review of the manuscript. We thank the staff at The Genome Technology Center at NYU Grossman School of Medicine. This shared resource is partially supported by the Cancer Center Support Grant P30CA016087 at the Laura and Isaac Perlmutter Cancer Center. This research was supported by NYU Grossman School of Medicine (to S.A.L.), the Gifford Family Neuroimmune Consortium as part of the Cure Alzheimer's Fund (to S.A.L.), the Blas Frangione Foundation (to S.A.L.), Alzheimer's Research UK (to S.A.L.) and generous

anonymous donors (to S.A.L.). Additional support was from the Neurodegenerative Diseases Consortium from MD Anderson (to P.H. and S.A.L.). J.S.S. was supported by the National Institutes of Health (T32 via T32AG052909 (Wisniewski, Scharfman)). Additionally, S.A.L. and J.S.S. were supported by the Alzheimer's Disease Resource Center at NYU Langone Medical Center. This work was also supported, in part, by an unrestricted grant from Research to Prevent Blindness. We thank NanoString for gifting nCounter Glial Profiling Panel chips and reagents and for advice on analysis using the ROSALIND platform.

Author contributions

P.H., J.S.S., R.D.K. and I.V.L.R. conducted experiments. P.H. analyzed data. P.H. and S.A.L planned experiments. P.H. and S.A.L. prepared the manuscript. All authors approve of the final version of the manuscript.

Competing interests

S.A.L. is a founder of AstronauTx Ltd. All other others declare no competing financial interests.

Additional information

Extended data is available for this paper at https://doi.org/10.1038/s41593-021-00905-6.

Supplementary information The online version contains supplementary material available at https://doi.org/10.1038/s41593-021-00905-6.

Correspondence and requests for materials should be addressed to P.H. or S.A.L.

Peer review information *Nature Neuroscience* thanks the anonymous reviewers for their contribution to the peer review of this work.

Reprints and permissions information is available at www.nature.com/reprints.

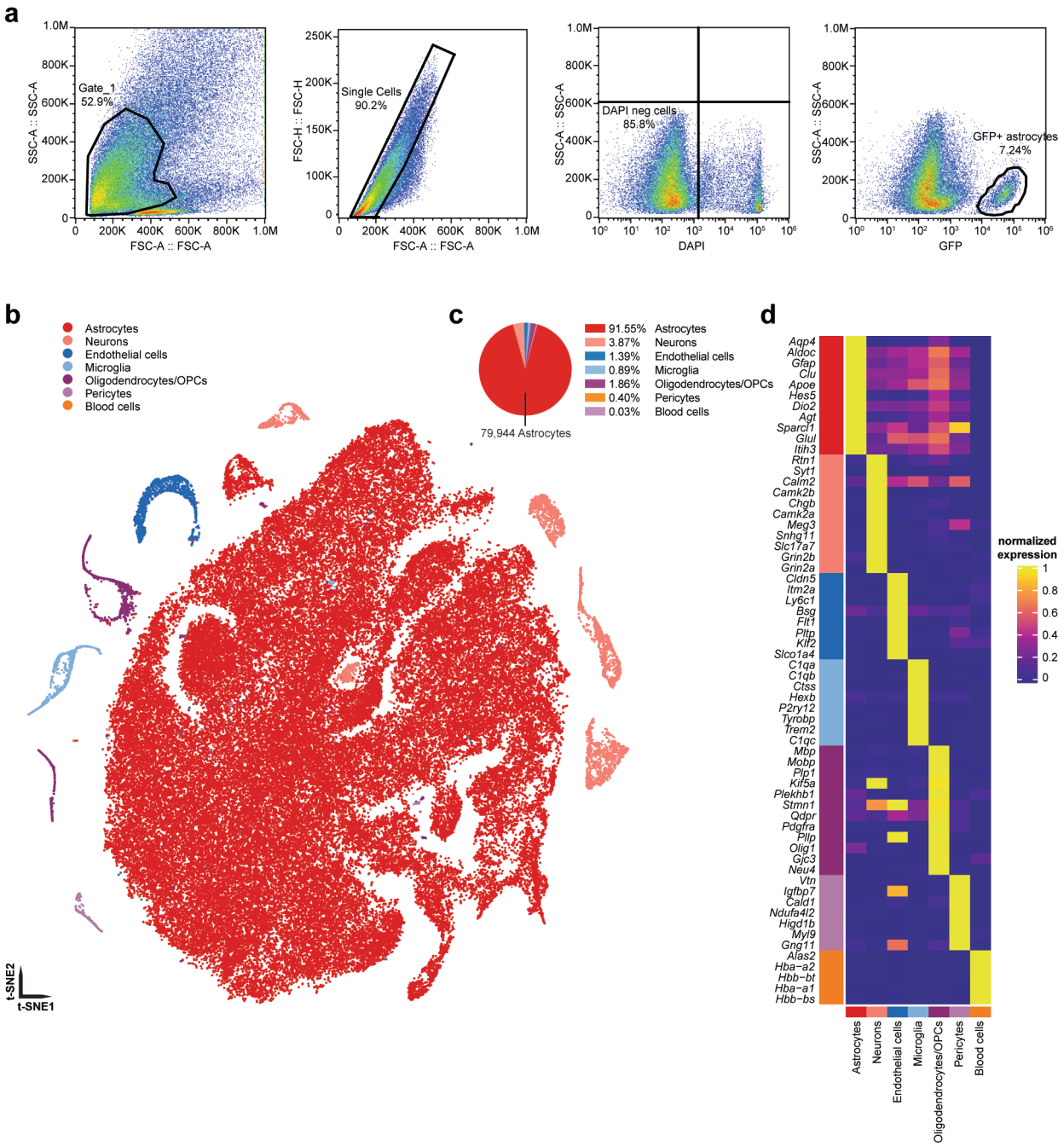

Extended Data Fig. 1 | FACS strategy to purify GFP + astrocytes from Aldh1l1^{eGFP} mice, initial clustering and cell type identification. a, A single cell suspension of mouse cortex was prepared (see Methods) and cells from two hemispheres were recovered in 500 µL 1%BSA containing PBS. Cells were run on a Sony SH800Z with a 100 µm nozzle at 4 °C. Gating was set to capture single cells that were DAPI-negative (alive) and GFP-positive (astrocytes). 100.000 GFP + astrocytes were captured per mouse. Channels were: DAPI (405 nm) and GFP (488 nm). Abbreviations: SSC, side scatter; FSC, forward scatter, a, area; w, width. **b,c**, Initial clustering of all 91110 cells across all 12 animals identifies presence and percentage of non-astrocytic cells as defined by cell type marker genes in (**d**). **d**, Heatmap of normalized cell type marker genes across the identified cell type clusters.

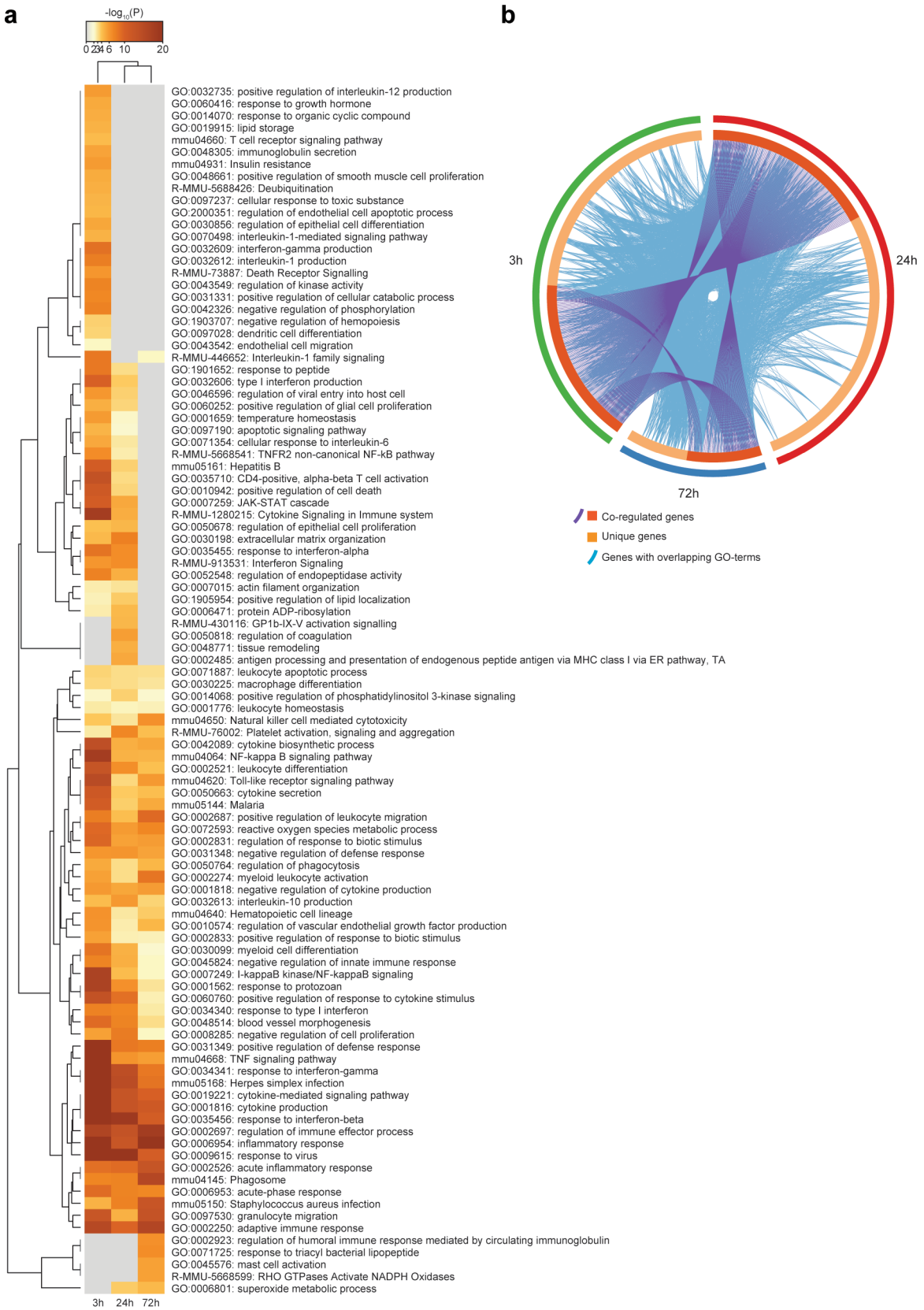

Extended Data Fig. 2 | Gene Ontology (GO) analysis of LPS-induced genes at 3 h, 24 h and 72 h after injection. a, Genes induced ≥1 log2 fold at each time point with *padj* < 0.05 were used to perform GO-term analysis using Metascape[18]. Shown are the top 100 GO terms according to p-value and clustered by p-value at each time point. **b**, Shown are genes induced ≥1 log2 fold with *padj* < 0.05 for each time point (light and dark orange). Light orange are genes unique to the time point, dark orange are genes co-regulated at at least two time points. Dark blue lines connect genes that are co-regulated. Light blue lines connect genes with overlapping GO-terms.

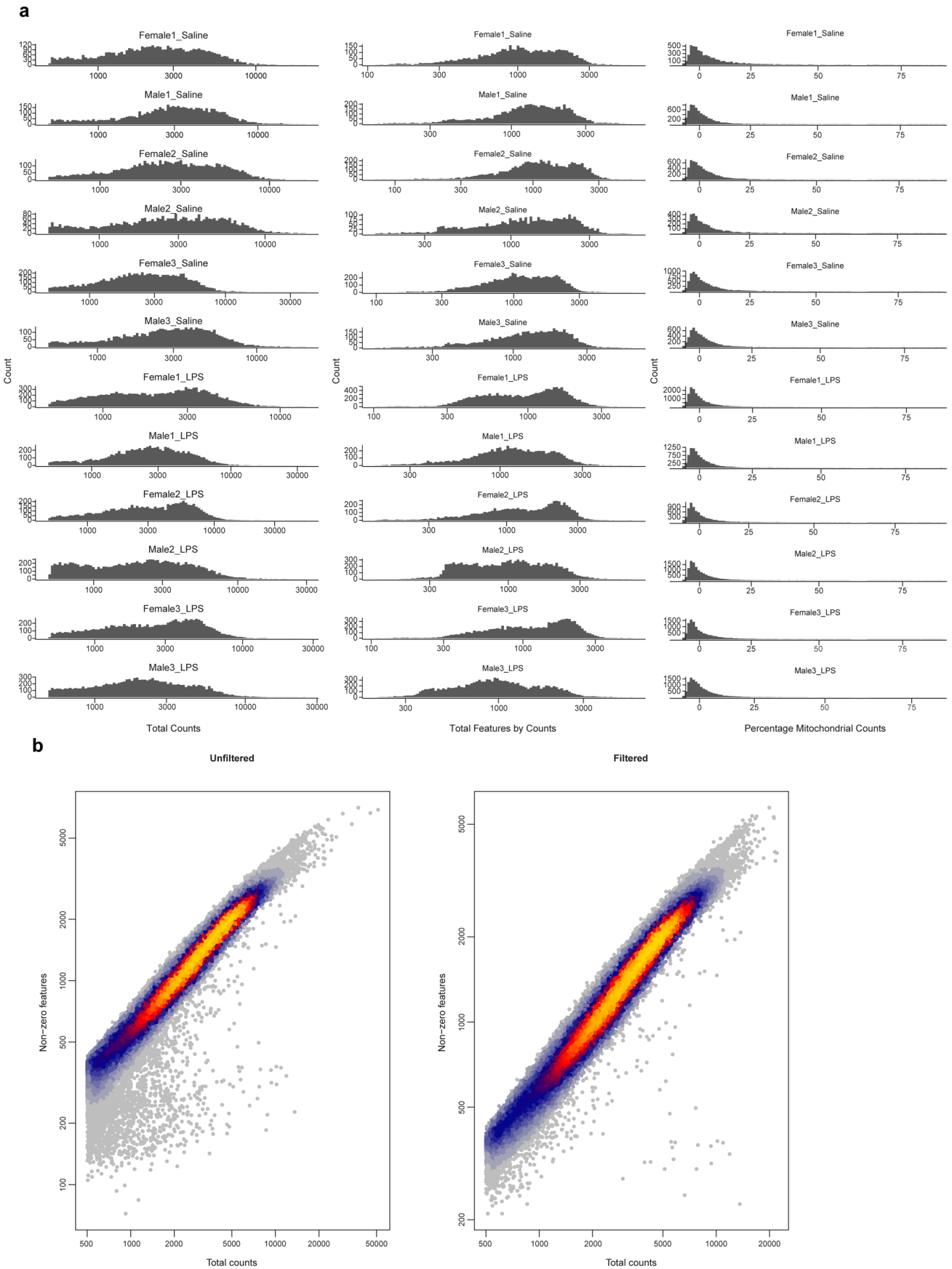

Extended Data Fig. 3 | Filtering of scRNAseq samples based on per sample count data. a, Histograms showing total counts, total features per counts as well as the percentage of mitochondrial counts for each of the 12 single-cell RNA-seq samples. **b**, Scatter plot showing total counts (x-axis) and total features by counts (y-axis) before and after filtering.

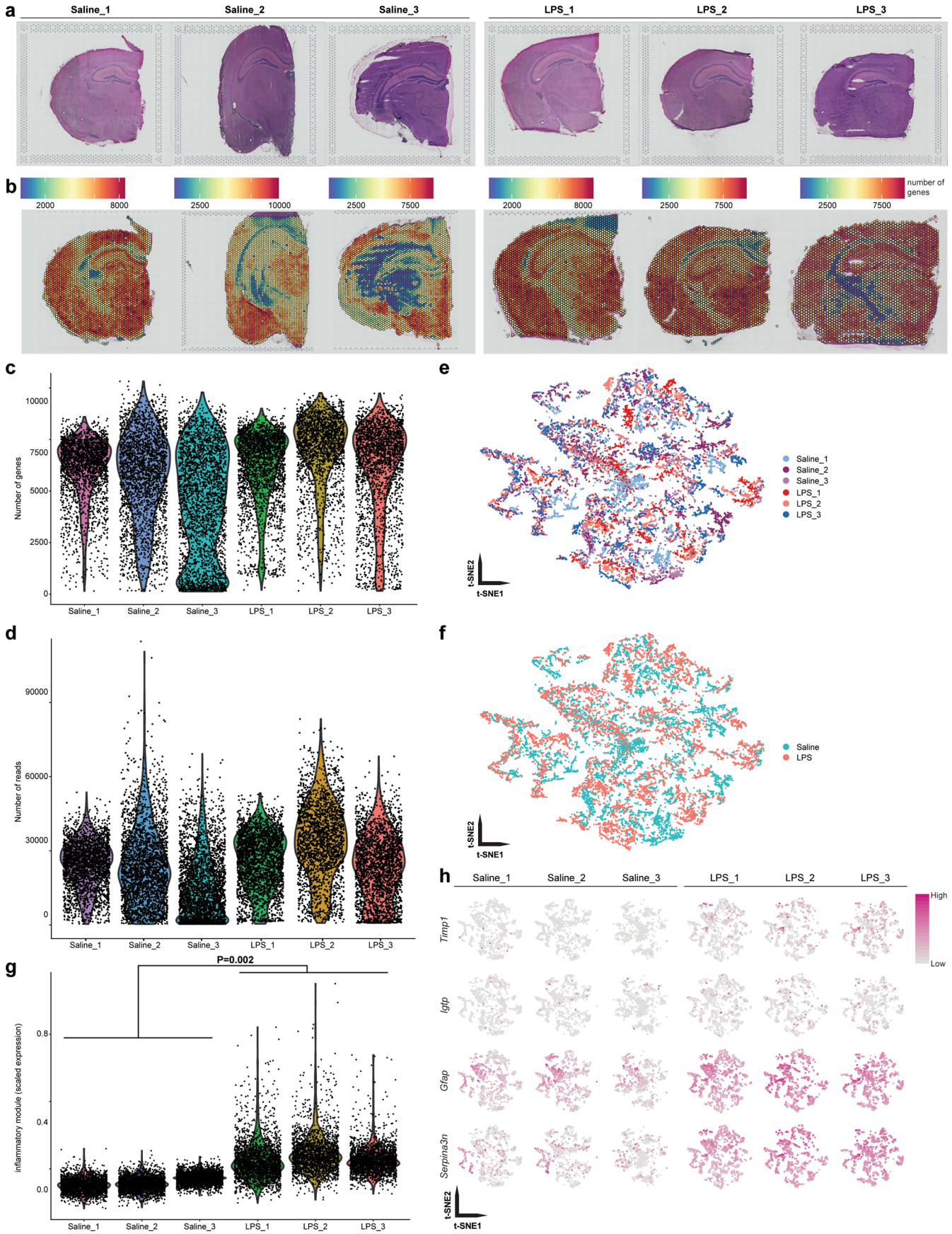

Extended Data Fig. 4 | See next page for caption.

Extended Data Fig. 4 | QC and validation of six Visium spatial transcriptomics sections from saline- and LPS-treated animals. a, H&E staining of 10 µm coronal sections from three saline-treated and three LPS-treated mice. **b**, FeaturePlot showing number of genes across all tissue covered spots across the six brains sections. **c**, Violin plot quantifying the FeatuePlot in (**b**) showing the number of genes across the six brain sections. **d**, Violin plot showing the number of reads per brain section. **e**, t-SNE of the six brain sections, three saline- and three LPS-treated. Each dot represents one spot of a Visium Gene Expression Slide capture area. **f**, t-SNE as in (**e**) but with saline- and LPS-treated animals grouped. **g**, Violin plot highlighting an inflammatory module created from the top LPS-responsive genes shows inflammatory gene induction in brain sections from LPS- but not saline-treated animals (* = $p < 0.05$, two-tailed t-test on spot-averages of inflammatory gene modules). **h**, FeaturePlots showing expression of *Timp1*, *Igtp*, *Gfap* and *Serpina3n* across the six brain sections.

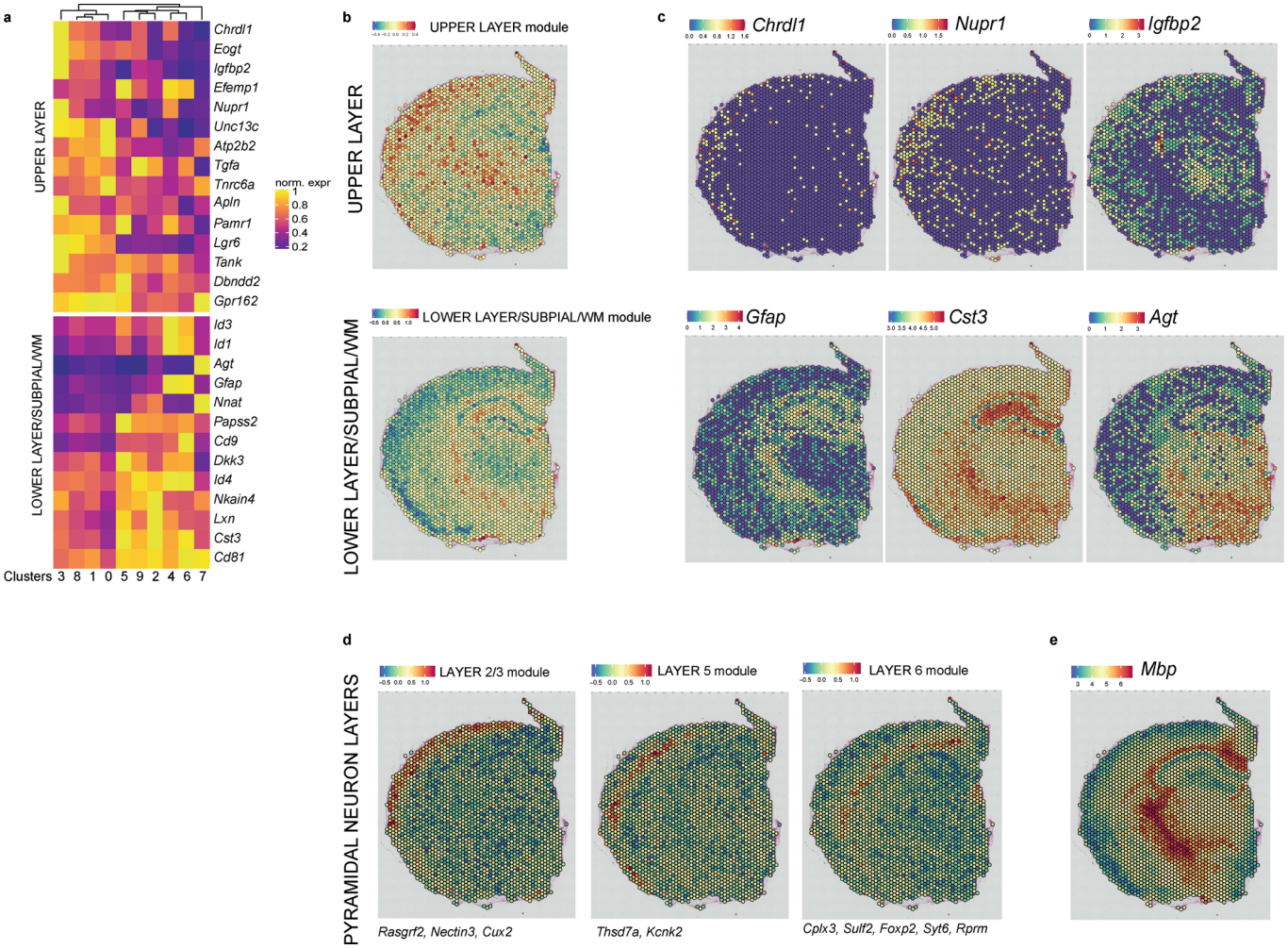

Extended Data Fig. 5 | Astrocytic subtypes differentially express layer-specific genes that can be found in brain sections using spatial transcriptomics. **a**, Heatmap showing normalized cluster averages of upper layer or lower layer/subpial/white matter astrocyte genes as identified in Bayraktar et. al. 2020[10]. **b**, Identification of brain location of upper layer or lower layer/subpial/white matter astrocytes using modules of layer-specific genes using Visium spatial transcriptomics (**a**). **c**, Example genes from (**a**) shows the gene distribution of upper versus lower layer/subpial/white matter genes across the coronal brain section. **d**, Layer-specific pyramidal neuron genes were taken from scRNA-seq data from Zeisel et. al. 2015[12], subset into modules and highlighted in a coronal Visium section from a saline-treated animal. **e**, Visium showing the expression of *Mbp* to highlight presence of white matter tracts in the coronal brain section.

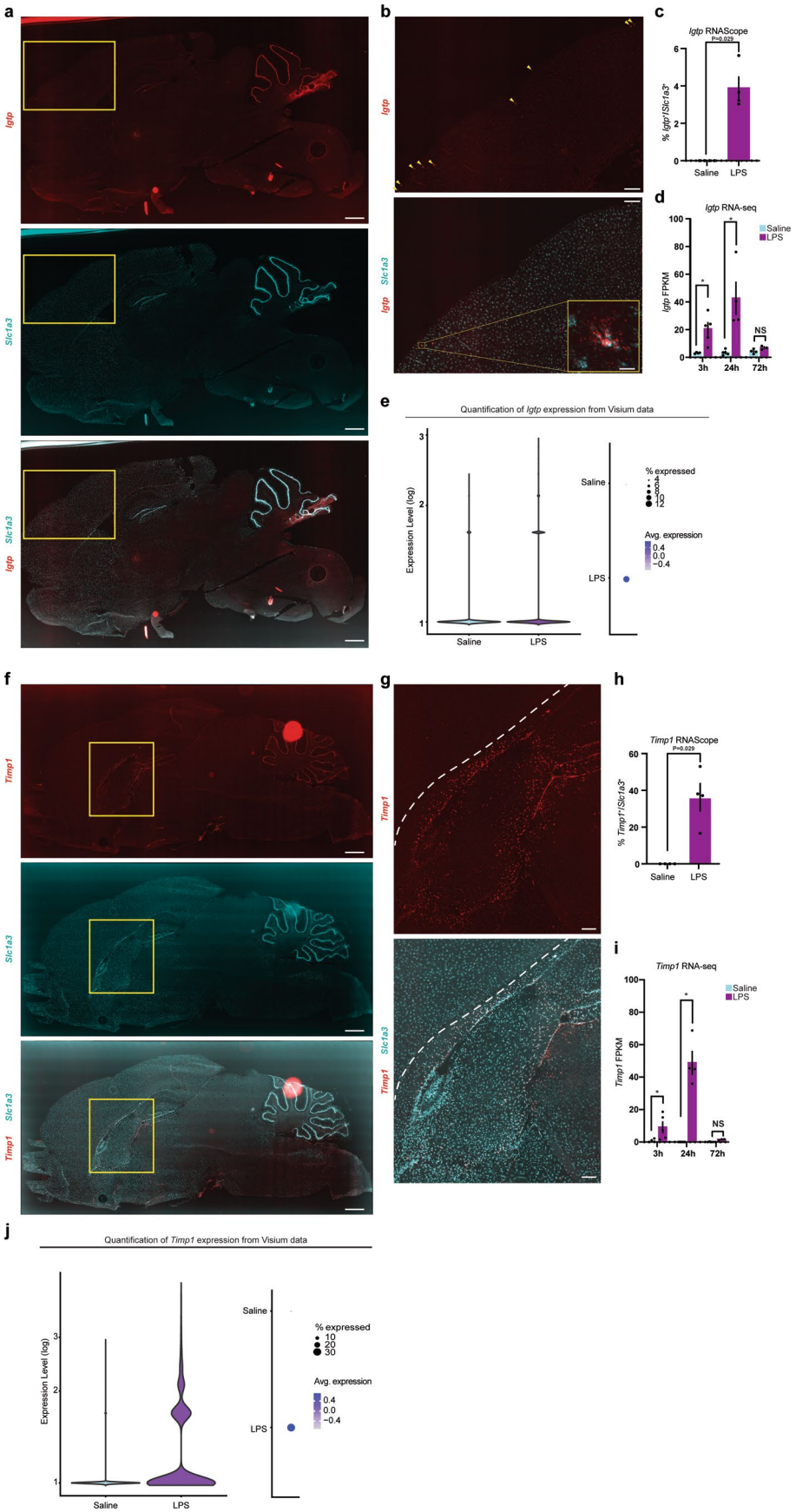

Extended Data Fig. 6 | See next page for caption.

Extended Data Fig. 6 | Multimodal quantification of Cluster 8 gene *Igtp* and Cluster 4 gene *Timp1*. a, Representative sagittal section from female P30 mouse 24 h after LPS injection highlighting *Igtp* (red, top), *Slc1a3* (cyan, middle) and co-localization (bottom) using RNAScope based on 4 saline- and 4 LPS-injected animals. Scale bar = 250 μm. **b**, Magnification of area in (**a**) indicated by yellow box. Yellow arrows indicate *Igtp* + astrocytes in Layer1 and surface of the brain. Scale bar = 100 μm. Inset shows a magnification of a single *Igtp* + astrocyte. Scale bar = 10 μm **c**, Quantification of *Igtp* + */Slc1a3* + astrocyte numbers using RNAScope in Layer1 of the cortex. A cell is identified as *Igtp* + if it expresses ≥20 dots/cell. P-value calculated with Mann-Whitney test, n = 4 saline-treated mice, n = 4 LPS-treated mice, 2-3 sections per mouse. Bar graphs show the mean, error bars SEM. **d**, *Igtp* expression in FACS-purified astrocytes 3 h (n = 4 saline, 5 LPS), 24 h (n = 5 saline, 4 LPS) and 72 h (n = 4 saline, 3 LPS) after LPS injection. * = padj<0.05, DESeq2, compared to corresponding saline-injected mice. Exact padj values can be found in Supplementary Table 1. N indicates number of animals, bar graphs show the mean, error bars are SEM. **e**, *Igtp* expression as quantified with Visium. Log *Igtp* levels (left) and percentage of spots with detectable *Igtp* levels as well as scaled average expression (right), across all spots from 3 saline- and 3 LPS-treated animals. **f**, Representative sagittal section from female P30 mouse 24 h after LPS injection highlighting *Timp1* (red, top), *Slc1a3* (cyan, middle) and co-localization (bottom) using RNAScope based on 4 saline- and 4 LPS-injected animals. Scale bar = 250 μm. **g**, Magnification of area in (**f**) indicated with a yellow box. White dashed line demarcates transition from white to gray matter. Scale bar = 50 μm. **h**, Quantification of *Timp1* + */Slc1a3* + astrocyte numbers using RNAScope in corpus callosum. A cell is identified as *Timp1* + if it expresses ≥20 dots/cell. P-value calculated with Mann-Whitney test, n = 4 saline-treated mice, n = 4 LPS-treated mice, 2-3 sections per mouse. Bar graphs show the mean, error bars SEM. **i**, *Timp1* expression in FACS-purified astrocytes 3 h (n = 4 saline, 5 LPS), 24 h (n = 5 saline, 4 LPS) and 72 h (n = 4 saline, 3 LPS) after LPS injection. * = padj<0.05, DESeq2, compared to corresponding saline-injected mice. Exact padj values can be found in Supplementary Table 1. N indicates number of animals, bar graphs show the mean, error bars are SEM. **e**, *Timp1* expression as quantified with Visium. Log *Timp1* levels (left) and percentage of spots with detectable *Igtp* levels as well as scaled average expression (right), across all spots from 3 saline- and 3 LPS-treated animals.

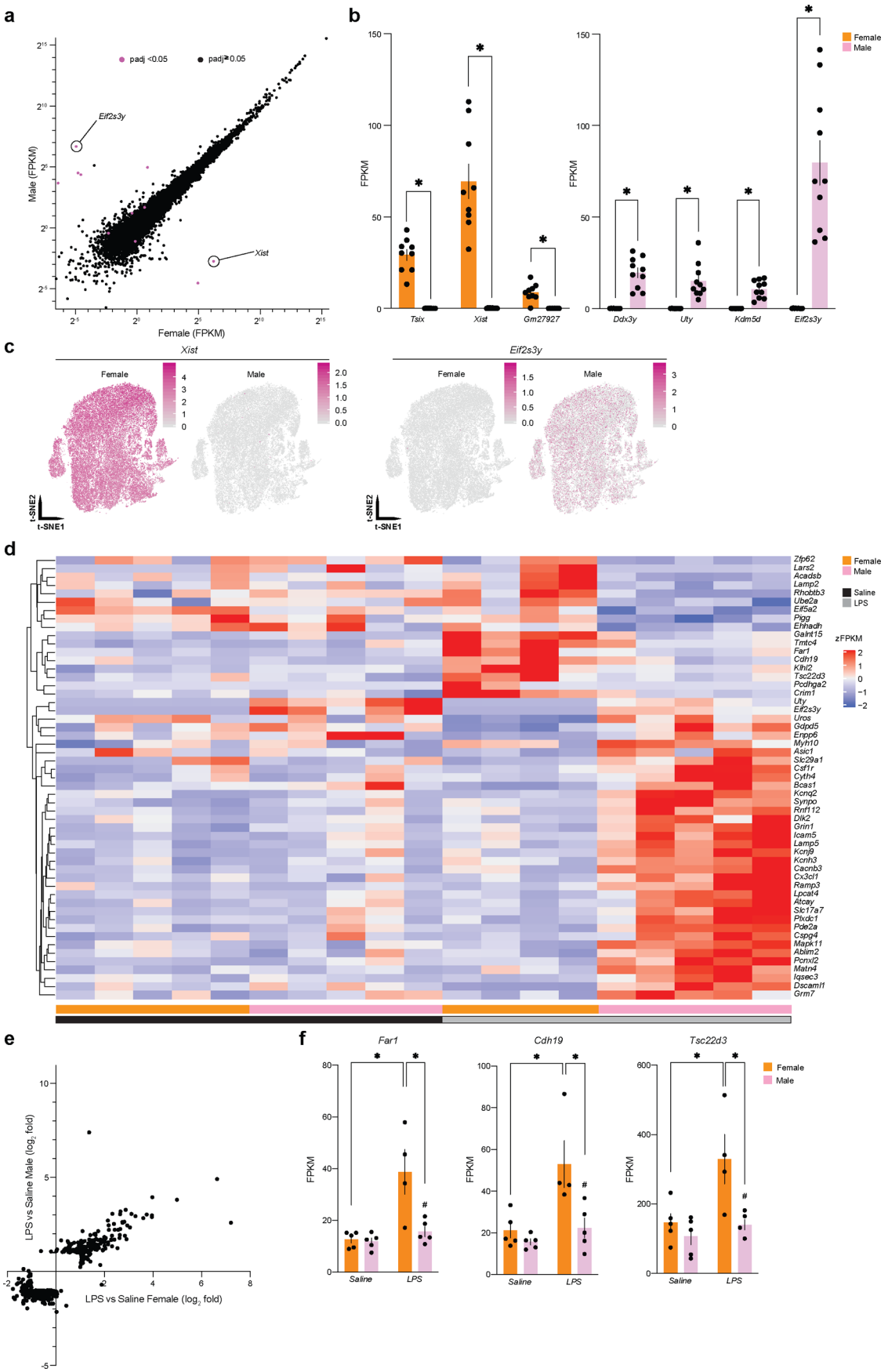

Extended Data Fig. 7 | See next page for caption.

Extended Data Fig. 7 | There are few sex-specific differences in astrocytic gene expression during inflammation. a, FPKM scatter plot showing all genes expressed >0.5 FPKM in astrocytes purified from male and female saline-injected Aldh1l1^{eGFP} mice based on bulk sequencing. Genes that are differentially expressed with *padj* < 0.05 are highlighted in purple. Circled are the highest expressed genes according to FPKM specific to males and females, *Eif2s3y* and *Xist*, respectively. **b**, Bar graphs showing mean FPKM values of genes differentially expressed (* = padj<0.05, DESeq2) between male (n = 10) and female mice (n = 9). Circles are single animals, error bars are SEM. **c**, t-SNE feature plot highlighting female-specific gene *Xist* and male-specific gene *Eif2s3y*. **d**, Heatmap showing z-normalized FPKM levels of sex-specific LPS-induced genes. **e**, Scatter plot comparing log2 fold inductions due to LPS compared to saline-injected mice based on bulk sequencing. Genes included are >10 FPKM and padj<0.05 in either males or females as a consequence of LPS injection. **f**, Bar graphs showing mean FPKM values of example genes only induced in female mice (* = *padj* < 0.05, # = NS compared to male saline, DESeq2) *Far1*, *Cdh19* and *Tsc22d3*. Circles are single animals, error bars are SEM.

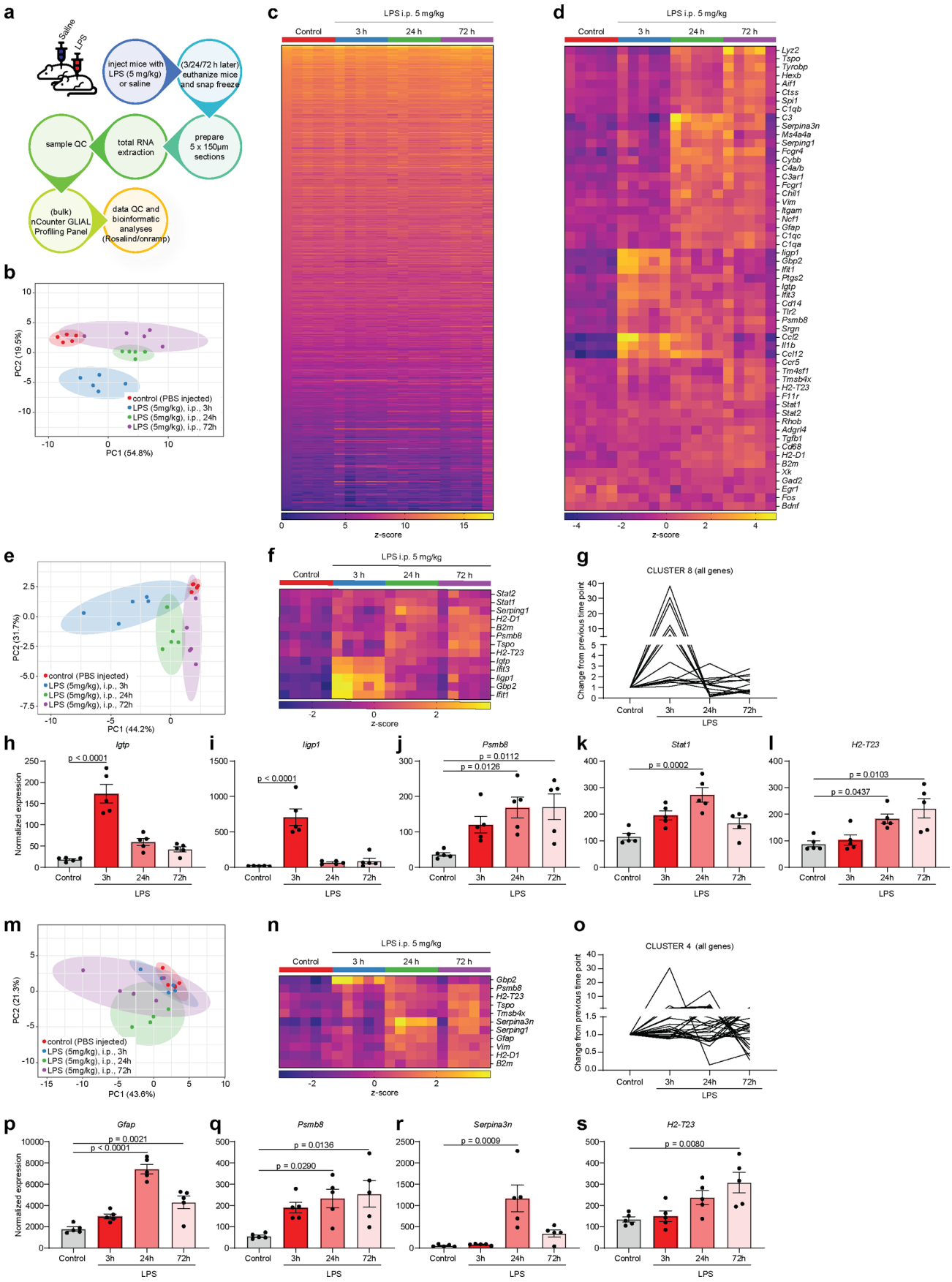

Extended Data Fig. 8 | See next page for caption.

Extended Data Fig. 8 | Nanostring® Glial Profiling Panel was used to validate lowly abundant transcripts discovered using single cell RNASeq experiments. a, Schematic for Nanostring Glial Profile Panel experiments. Brain sections from P30 Aldh1l1^{eGFP} mice injected with saline or lipopolysaccharide (LPS) were collected at 3, 24, or 72 h. **b**, Principle Component (PC) plot of all samples. **c**, Heatmap of expression level z-scores for 720 genes included in Panel across time since LPS injection. **d**, Heatmap of z-scores of differentially expressed genes following LPS injection. **e**, PC plot of genes identified from single cell RNA sequencing (scRNASeq) experiments and enriched in Cluster 8. **f**, Heatmap of Cluster 8 enriched transcripts. **g**, Fold-change in expression of Cluster 8 enriched genes with time following LPS injection (compared to the previous time point). **h-l**, Bar plots showing raw expression values (normalized to chip control transcripts) for individual genes enriched in Cluster 8 (error bars are SEM). While many genes are enriched by 3 h and have lowered expression levels by 24 h, for example *Igtp* (**h**), *Iigp1* (**i**), others maintain increased expression for several days (**j-l**).n = 5 animals per condition. **m**, PC plot of genes identified from scRNASeq experiments and enriched in Cluster 4. **n**, Heatmap of Cluster 4 enriched transcripts. N = 5 biological replicates per group. **o**, Fold-change in expression of Cluster 4 enriched genes with time following LPS injection (compared to the previous time point). **p-s**, Bar plots showing raw expression values (normalized to Nanostring chip control transcripts) for individual genes enriched in Cluster 4 (error bars are SEM). Abbreviations: LPS, lipopolysaccharide; PC, principle component; QC, quality control (bioAnalyzer chip); scRNASeq, single cell RNA sequencing = 5 biological replicates per group. Prediction ellipses in b,e,m represent probability = 0.95.

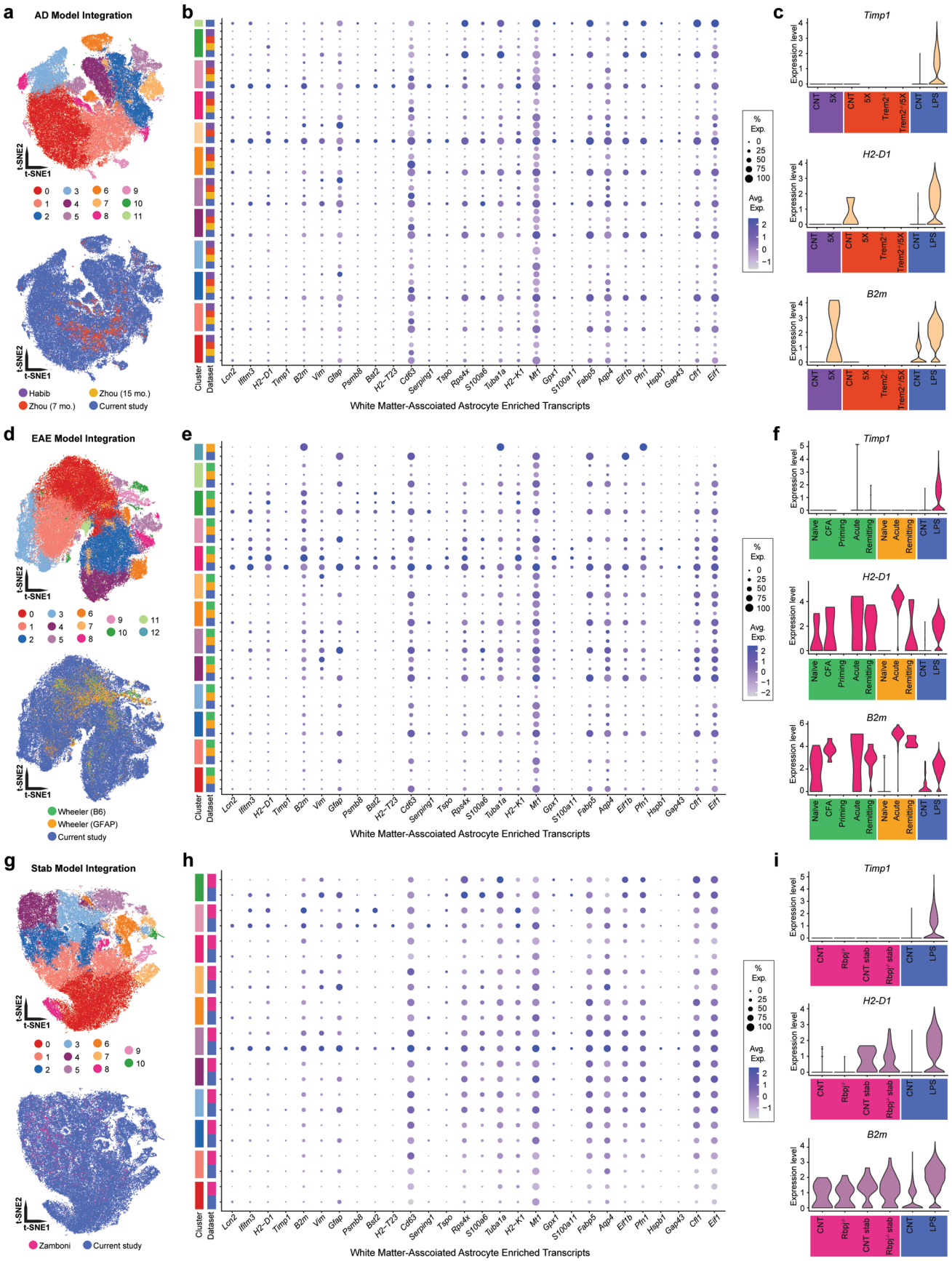

Extended Data Fig. 9 | See next page for caption.

Extended Data Fig. 9 | White matter-associated astrocytes are not well-defined in integrated datasets. Integration of current study with published astrocyte datasets to visualize white matter-associated astrocytes **a**, t-SNE projection of 89,420 astrocytes identified by unique astrocyte clusters (top) and original dataset (bottom). **b**, Dotplot showing genes enriched in white matter-associated astrocytes, split by dataset and cluster. Data: 5xFAD[34] (purple), Trem2$^{-/-}$/5xFAD[35] 7-month (red) and 15-month (yellow), and current study (blue). **c**, Violin plots of white matter-associated astrocyte transcripts split by dataset and disease. Only data from integrated cluster 7 (that is, integrated white matter-associated astrocyte subpopulation) are visualized. **d**, t-SNE projection of 100,471 astrocytes identified by unique astrocyte clusters (top) and original dataset (bottom). **e**, Dotplot showing genes enriched in white matter-associated astrocytes, split by dataset and cluster. Data: EAE from two isolated populations[36] - one un-sorted (green) and the other *Gfap*^{TdT}-sorted (orange), and current study (blue). **f**, Violin plots of white matter-associated astrocyte transcripts split by dataset and disease. Only data from integrated cluster 8 (that is, integrated white matter-associated astrocyte subpopulation) are visualized. **g**, t-SNE projection of 83,684 astrocytes identified by unique astrocyte clusters (top) and original dataset (bottom). **h**, Dotplot showing genes enriched in white matter-associated astrocytes, split by dataset and cluster. Data: stab wound[37] (pink) and current study (blue). **i**, Violin plots of white matter-associated astrocyte transcripts split by dataset and model. Only data from integrated cluster 5 (that is, integrated white matter-associated astrocyte subpopulation) are visualized. Abbreviations: 5X, 5xFAD; AD, Alzheimer's disease; B6, C57BL/6 J mice; CNT, control; EAE, experimental autoimmune encephalomyelitis; LPS, lipopolysaccharide; CFA, complete Freund's adjuvant.

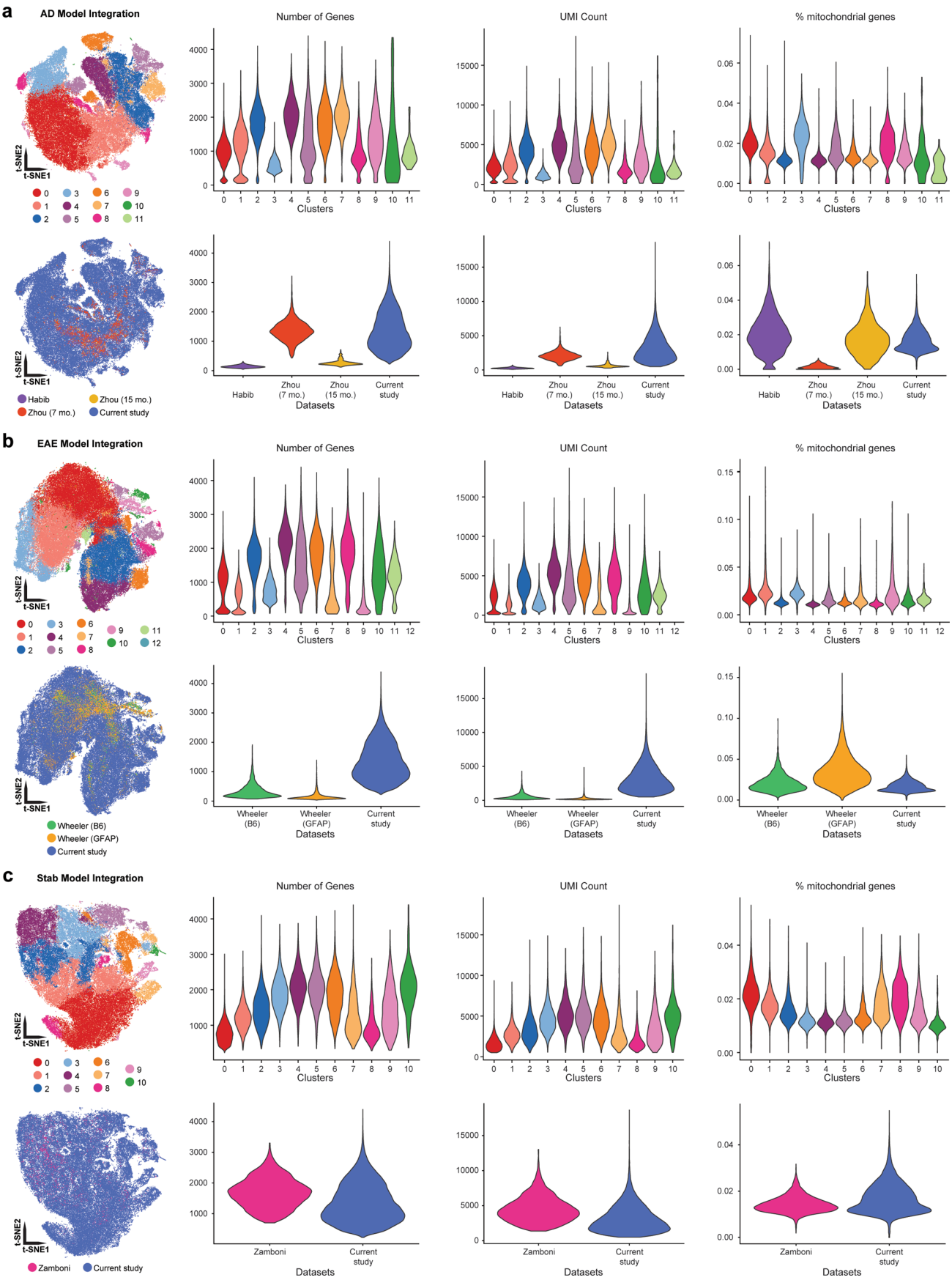

Extended Data Fig. 10 | See next page for caption.

Extended Data Fig. 10 | Dataset quality assessment: Genes, UMI counts, and percentage of mitochondrial genes per cell split by cluster and by dataset. t-SNE projections of astrocytes and violin plots of quality control metrics for AD models (5xFAD, Trem2$^{-/-}$, and Trem2$^{-/-}$/5xFAD) (**a**), a model of demyelination (experimental autoimmune encephalomyelitis, EAE) (**b**), and an acute injury/stab wound model (**c**) split by astrocyte cluster (top) and by dataset (bottom). Habib et al. (2020 – 5xFAD)[34] data are in purple, Zhou et al. (2020 – 5xFAD, Trem2$^{-/-}$, and Trem2$^{-/-}$/5xFAD)[35] 7-month time point data are in red, Zhou et al. (2020 – 5xFAD) 15-month time point data are in yellow, Wheeler et al. (2020 – EAE)[36] B6 sample data are in green, Wheeler et al. (2020 – EAE) *TdTomato*^{GFAP}-sorted sample data are in orange, Zamboni et al. (2020 – stab wound)[37] data are in pink, and the current study data (acute inflammation using lipopolysaccharide, LPS) are in blue. Abbreviations: AD, Alzheimer's disease; B6, C57BL/6 J mice; GFAP, *TdTomato*^{GFAP} mice; EAE, experimental autoimmune encephalomyelitis; LPS, lipopolysaccharide; Trem2$^{-/-}$, Trem2 knockout mice; Trem2$^{-/-}$/5X, Trem2 knockout 5xFAD mice; UMI, unique molecular identifier.

nature research

Corresponding author(s): Philip Hasel, Shane Liddelow

Last updated by author(s): 06/03/2021

Reporting Summary

Nature Research wishes to improve the reproducibility of the work that we publish. This form provides structure for consistency and transparency in reporting. For further information on Nature Research policies, see Authors & Referees and the Editorial Policy Checklist.

Statistics

For all statistical analyses, confirm that the following items are present in the figure legend, table legend, main text, or Methods section.

n/a	Confirmed
☐	☒ The exact sample size (*n*) for each experimental group/condition, given as a discrete number and unit of measurement
☐	☒ A statement on whether measurements were taken from distinct samples or whether the same sample was measured repeatedly
☐	☒ The statistical test(s) used AND whether they are one- or two-sided *Only common tests should be described solely by name; describe more complex techniques in the Methods section.*
☐	☒ A description of all covariates tested
☐	☒ A description of any assumptions or corrections, such as tests of normality and adjustment for multiple comparisons
☐	☒ A full description of the statistical parameters including central tendency (e.g. means) or other basic estimates (e.g. regression coefficient) AND variation (e.g. standard deviation) or associated estimates of uncertainty (e.g. confidence intervals)
☐	☒ For null hypothesis testing, the test statistic (e.g. *F*, *t*, *r*) with confidence intervals, effect sizes, degrees of freedom and *P* value noted *Give P values as exact values whenever suitable.*
☒	☐ For Bayesian analysis, information on the choice of priors and Markov chain Monte Carlo settings
☒	☐ For hierarchical and complex designs, identification of the appropriate level for tests and full reporting of outcomes
☒	☐ Estimates of effect sizes (e.g. Cohen's *d*, Pearson's *r*), indicating how they were calculated

Our web collection on statistics for biologists contains articles on many of the points above.

Software and code

Policy information about availability of computer code

Data collection

Sequencing:NovaSeq 6000 RTA v3.4.4 (basecalling); bcl2fastq Conversion software v2.20 (FASTQ generation)
Microscope: Keyence BZ-X710 Image Acquisition Software
FACS: Sony SH800Z software

Data analysis

scds 1.1.2
scater v1.13.23
SpaceRanger v1.2.0
edgeR v3.27.13
Cell Ranger v3.0.2
CATALYST 1.9.8
UpSetR 1.4.0
ComplexHeatmap v2.1.0
OnRamp
ggplot2 v3.2.1
dplyr v0.8.3
purrr v0.3.3
RColorBrewer v1.1-2
viridis v0.5.1
scran v1.13.25
Seurat v3.1.0
SingleCellExperiment v1.7.11

muscat v0.99.9
circlize v0.4.8
VennDiagram v1.6.20
HISAT2 v.2.1.0
StringTie v2.1.1
DESeq2 v2.11.40.6
Prism8 v8.2.1
Microsoft Excel v16.14.1
ImageJ/Fiji v2.0.0-rc-69/1.52p
LSD v4.0-0

For manuscripts utilizing custom algorithms or software that are central to the research but not yet described in published literature, software must be made available to editors/reviewers. We strongly encourage code deposition in a community repository (e.g. GitHub). See the Nature Research guidelines for submitting code & software for further information.

Data

Policy information about availability of data

All manuscripts must include a data availability statement. This statement should provide the following information, where applicable:

- Accession codes, unique identifiers, or web links for publicly available datasets
- A list of figures that have associated raw data
- A description of any restrictions on data availability

All sequencing data generated in association with this study are available in the Gene Expression Omnibus as a SuperSeries under accession number GSE148612. Mouse scRNASeq is available under accession number GSE148611, mouse bulk RNASeq is available under accession number GSE148610, mouse spatial transcriptomic under GSE165098 and rat bulk RNAseq data is available under accession number GSE165069.
Bulk sequencing of in vivo mouse astrocytes, in vivo mouse astrocyte scRNAseq pseudobulk and in vitro rat astrocyte bulk RNAseq are available to search on www.gliaseq.com. scRNASeq at single cell resolution as well as spatial transcriptomic data are available on www.gliaseqpro.com. NanoString data is available on https://rosalind.onramp.bio/showcase/liddelow
scRNASeq data from other studies referenced in Fig. 7 and Extended Data Fig 9, 10, are available from the Gene Expression Omnibus under accession numbers GSE143758, GSE140511, GSE130119 and GSE139842.
Details of analysis pipeline libraries are listed in Methods and available at https://github.com/liddelowlab/Hasel_et_al.

All supplemental tables with processed data have been submitted with this manuscript.

Field-specific reporting

Please select the one below that is the best fit for your research. If you are not sure, read the appropriate sections before making your selection.

☒ Life sciences ☐ Behavioural & social sciences ☐ Ecological, evolutionary & environmental sciences

For a reference copy of the document with all sections, see nature.com/documents/nr-reporting-summary-flat.pdf

Life sciences study design

All studies must disclose on these points even when the disclosure is negative.

Sample size	N numbers range from n=3 to n=5, with n= individual mouse, based on previously published work using the same stimulation paradigm and readout (PMID:22553043).
Data exclusions	No data was excluded from the analysis
Replication	For scRNAseq, 6 animals were used per condition (saline vs LPS) leading to 12 independent samples and single cell reactions. For in vivo and in vitro astrocyte bulk RNAseq, 3-5 independent biological replicates (animals) were used and sequenced per condition. For NanoString, 5 independent biological replicates (animals) were used per time point. For RNAScope, 4 animals were used per condition (saline vs LPS) with 2-3 sections per animal.
Randomization	Animals were randomly assigned to be either injected with saline or LPS as long as they made age and sex criteria, and the stimulation time points were collected over several months to avoid batch effects
Blinding	Due to the nature of the physiological response to LPS, animals that received injection and immediately noticeable even at 3h. For this reason, even when blinded, the experimenter is aware of which animals received injections of LPS. For all other analyses, the experimenter was blinded to the genotype or treatment until completion of statistical analyses.

Reporting for specific materials, systems and methods

We require information from authors about some types of materials, experimental systems and methods used in many studies. Here, indicate whether each material, system or method listed is relevant to your study. If you are not sure if a list item applies to your research, read the appropriate section before selecting a response.

Materials & experimental systems

n/a	Involved in the study
☒	☐ Antibodies
☒	☐ Eukaryotic cell lines
☒	☐ Palaeontology
☐	☒ Animals and other organisms
☒	☐ Human research participants
☒	☐ Clinical data

Methods

n/a	Involved in the study
☒	☐ ChIP-seq
☐	☒ Flow cytometry
☒	☐ MRI-based neuroimaging

Animals and other organisms

Policy information about studies involving animals; ARRIVE guidelines recommended for reporting animal research

Laboratory animals	For all in vivo experiments, P30-35 'Aldh1l1eGFP' (Tg(Aldh1l1-EGFP)OFC789Gsat/Mmucd, RRID:MMRRC_011015-UCD) mice were used. For in vitro culture work, P5 Sprague Dawley rat pups (Charles River, Strain Code 400) were used. Both sexes.All animals were housed at 22–25 °C/50-60% humidity on a 12-h light/dark cycle (light on 6:00) with water and food provided ad libitum.
Wild animals	Study did not involve wild animals
Field-collected samples	Study did not involve field-collected samples
Ethics oversight	All animal procedures were in accordance with the guidelines provided by the National Institute of Health as well as NYU Langone School of Medicine's Administrative Panel on Laboratory Animal Care.

Note that full information on the approval of the study protocol must also be provided in the manuscript.

Flow Cytometry

Plots

Confirm that:

☒ The axis labels state the marker and fluorochrome used (e.g. CD4-FITC).

☒ The axis scales are clearly visible. Include numbers along axes only for bottom left plot of group (a 'group' is an analysis of identical markers).

☒ All plots are contour plots with outliers or pseudocolor plots.

☒ A numerical value for number of cells or percentage (with statistics) is provided.

Methodology

Sample preparation	Animals were euthanized using CO2 and brains were immediately put into PBS for dissection. Cortices were removed from the rest of the brain, diced into 1 mm3 cubes and moved into enzyme solution (1xEBSS (Sigma, E7510), 0.46% Glucose (VWR, AAA16828- 0E), 26 mM NaHCO3 (Sigma, S4019), 0.5 mM EDTA (Sigma, 27285)) containing 200 Units of Papain per brain (Worthington Biochemical, LS003126) and incubated for 40 min at 37 °C with the tissue being agitated every 10 minutes. All solutions used throughout contained 125 Units DNAse/mL (Worthington Biochemical, LS002007). The brain tissue was then transferred into a canonical tube and after it settled, was washed three times with a trypsin inhibitor solution (1xEBSS (Sigma, E7510), 0.46% Glucose (VWR, AAA16828- 0E), 26 mM NaHCO3 (Sigma, S4019) in the presence of 1x Low-ovomucoid solution (10x stock: 15 mg/mL BSA (Sigma, A4161), 15 mg/ml ovomucoid (Worthington Biochemical, LS003086)). All following steps were performed either on wet ice or at 4 °C. After the last wash, cells were carefully triturated using a 2 mL serological pipette, letting non-homogenized tissue settle, and repeated twice more until most tissue was dissociated. The cells were transferred into a new canonical tube and a high ovomucoid solution (1xEBSS (Sigma, E7510), 0.46% Glucose (VWR, AAA16828- 0E), 26 mM NaHCO3 (Sigma, S4019) in the presence of 1x Hi-ovomucoid solution (10x stock: 30 mg/mL BSA (Sigma, A4161), 30 mg/ml ovomucoid (Worthington Biochemical, LS003086)) was carefully pipetted to the bottom of the tube. Cells were centrifuged at 400 g for 5 min at 4 °C and the pellet resuspended in 10 mL PBS (Invitrogen, 14190144). The cell suspension was then passed through a Nitex mesh filter (Nitex, 20 µM Tetko HC3-20) and then spun at 400 g for 5 min and resuspended in 500 µL PBS containing 1% BSA.
Instrument	Sony SH800Z
Software	System software that comes with Sony SH800Z
Cell population abundance	GFP+ astrocytes made up ~10% of DAPI-negative, single cell events , 100,000 astrocytes were collected per cortex

Gating strategy	Initial SSC/FSC was gated generously, followed by FSC-W/FSC-A to exclude doublets. DAPI positive cells were consider dead cells and a clear DAPI positive cell population was gated out. Finally, a very distinct GFP+ population emerged that was easily discernible from non-GFP+ cells

☒ Tick this box to confirm that a figure exemplifying the gating strategy is provided in the Supplementary Information.